AD-A037 192 ARMY ENGINEER WATERWAYS EXPERIMENT STATION VICKSBURG MISS F/G 13/2
LIQUEFACTION POTENTIAL OF DAMS AND FOUNDATIONS. REPORT 3. DEVEL--ETC(U)
FEB 77 G Y BALADI, B ROHANI

UNCLASSIFIED WES-RR-S-76-2-3 NL

| OF |
AD
A037192

END

DATE
FILMED
4-77

RESEARCH REPORT S-76-2

LIQUEFACTION POTENTIAL OF DAMS AND FOUNDATIONS

Report 3

DEVELOPMENT OF AN ELASTIC-PLASTIC CONSTITUTIVE RELATIONSHIP FOR SATURATED SAND

by

George Y. Baladi, Behzad Rohani

Soils and Pavements Laboratory
U. S. Army Engineer Waterways Experiment Station
P. O. Box 631, Vicksburg, Miss. 39180

February 1977
Report 3 of a Series

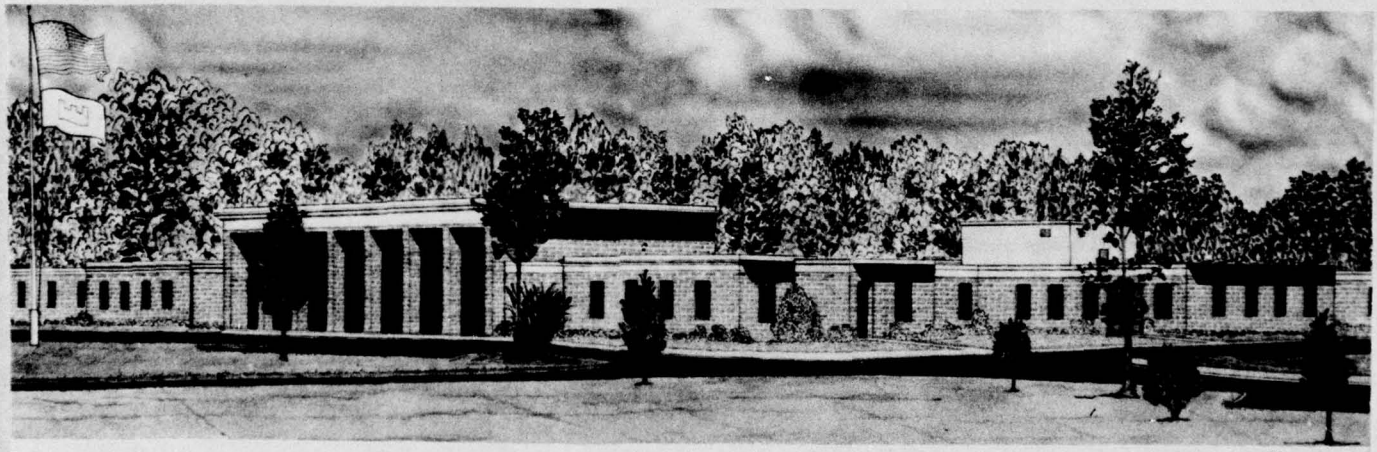

Prepared for Office, Chief of Engineers, U. S. Army
Washington, D. C. 20314

Under CWIS 31145

Destroy this report when no longer needed. Do not return it to the originator.

Unclassified

SECURITY CLASSIFICATION OF THIS PAGE (When Data Entered)

REPORT DOCUMENTATION PAGE

READ INSTRUCTIONS BEFORE COMPLETING FORM

1. REPORT NUMBER: Research Report S-76-2

2. GOVT ACCESSION NO.

3. RECIPIENT'S CATALOG NUMBER: Research rept.

4. TITLE (and Subtitle): LIQUEFACTION POTENTIAL OF DAMS AND FOUNDATIONS; Report 3, DEVELOPMENT OF AN ELASTIC-PLASTIC CONSTITUTIVE RELATIONSHIP FOR SATURATED SAND.

5. TYPE OF REPORT & PERIOD COVERED: Report 3 of a series

6. PERFORMING ORG. REPORT NUMBER: Sep 75—May 76

7. AUTHOR(s): George Y. Baladi, Behzad Rohani

8. CONTRACT OR GRANT NUMBER(s)

9. PERFORMING ORGANIZATION NAME AND ADDRESS: U. S. Army Engineer Waterways Experiment Station, Soils and Pavements Laboratory, P. O. Box 631, Vicksburg, Miss. 39180

10. PROGRAM ELEMENT, PROJECT, TASK AREA & WORK UNIT NUMBERS: CWIS 31145

11. CONTROLLING OFFICE NAME AND ADDRESS: Office, Chief of Engineers, U. S. Army, Washington, D. C. 20314

12. REPORT DATE: February 1977

13. NUMBER OF PAGES: 56 (61 p.)

14. MONITORING AGENCY NAME & ADDRESS (if different from Controlling Office): WES-RR-S-76-2-3

15. SECURITY CLASS. (of this report): Unclassified

15a. DECLASSIFICATION/DOWNGRADING SCHEDULE

16. DISTRIBUTION STATEMENT (of this Report)

Approved for public release; distribution unlimited.

17. DISTRIBUTION STATEMENT (of the abstract entered in Block 20, if different from Report)

18. SUPPLEMENTARY NOTES

19. KEY WORDS (Continue on reverse side if necessary and identify by block number)

Constitutive relations
Dams
Foundations
Liquefaction (soils)
Sands
Saturated soils

20. ABSTRACT (Continue on reverse side if necessary and identify by block number)

This report describes the initial attempt at developing a three-dimensional constitutive relationship for saturated sand. An isotropic constitutive relationship has been constructed, within the framework of the incremental theory of plasticity, that qualitatively simulates some of the features of the stress-strain-pore pressure response of saturated sand. It accounts for the hysteretic behavior of pressure-volumetric strain response of

(Continued)

DD FORM 1 JAN 73 1473 EDITION OF 1 NOV 65 IS OBSOLETE

Unclassified

SECURITY CLASSIFICATION OF THIS PAGE (When Data Entered)

038100

from

20. ABSTRACT (Continued).

sand, the effect of superimposed hydrostatic stress on shearing response, and the shear-induced volume change. It does not, however, treat strain-softening behavior and does not predict progressive increase of pore pressure under low-amplitude (subyield) cyclic loading conditions.

The behavior of the constitutive relationship under conventional undrained triaxial test condition is examined and correlated with experimental data for saturated Reid Bedford Model sand.

A recommendation is made that the present constitutive relationship be extended to quantitatively simulate the basic features of the stress-strain-pore pressure response of saturated sand, including the strain-softening behavior and the progressive increase of pore pressure observed under cyclic loading conditions.

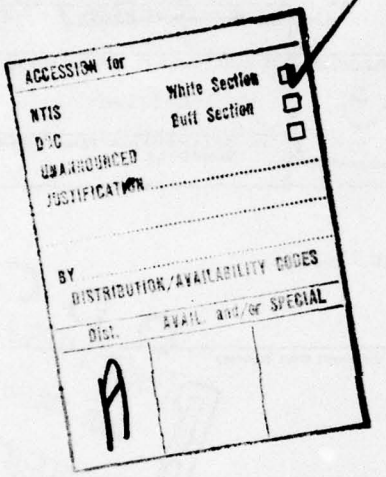

PREFACE

This investigation was conducted by the U. S. Army Engineer Waterways Experiment Station (WES) under the sponsorship of the Office, Chief of Engineers, Department of the Army, as a part of Project CWIS 31145, "Liquefaction Potential of Dams and Foundations Under Earthquake Excitation."

The investigation was conducted by Drs. G. Y. Baladi and B. Rohani during the period September 1975 through May 1976, under the general direction of Mr. J. P. Sale, Chief, Soils and Pavements Laboratory (S&PL), and Drs. J. G. Jackson, Jr., Chief, Soil Dynamics Division (SSD), F. G. McLean, Chief, Earthquake Engineering and Vibrations Division (EE&VD), and W. F. Marcuson, III, Project Leader (EE&VD). The report was written by Drs. Baladi and Rohani.

COL G. H. Hilt, CE, and COL J. L. Cannon, CE, were Directors of WES during the preparation of this report. Technical Director was Mr. F. R. Brown.

CONTENTS

CONVERSION FACTORS, U. S. CUSTOMARY TO METRIC (SI) UNITS OF MEASUREMENT

U. S. customary units of measurement used in this report can be converted to metric (SI) units as follows:

Multiply	By	To Obtain
pounds (force) per square inch	6894.757	pascals
tons (force) per square foot	95.76052	kilopascals
pounds (mass) per cubic foot	16.01846	kilograms per cubic metre

DEVELOPMENT OF AN ELASTIC-PLASTIC CONSTITUTIVE RELATIONSHIP FOR SATURATED SAND

PART I: INTRODUCTION

Background

1. Liquefaction may be defined as the "transformation of a granular material from a solid state to a liquefied state."[1] The process which leads to liquefaction in saturated soil is believed to be associated with an increase of pore pressure and, therefore, a concurrent decrease of intergranular stresses. Liquefaction, and subsequent flow, occur whenever the intergranular stresses and, consequently, the shearing strength of the material are substantially reduced. Experimentally it has been shown that liquefaction can occur under both monotonically increasing[2] and cyclic[3,4] loading conditions. The mechanism of liquefaction during cyclic loading, however, is believed to be somewhat different than that under monotonic-type loading.[5] For example, in conventional triaxial tests (saturated undrained condition), liquefaction under monotonic loading can occur only for very loose sand. Under cyclic loading, on the other hand, it is possible to achieve liquefaction for dense as well as loose materials.

2. Regardless of the loading condition, before a rational analysis of a liquefaction problem in saturated sand can be performed, a constitutive relationship describing the stress-strain-pore pressure response of the material must be available. The constitutive relationship must be expressed in three-dimensional geometry and be applicable to any state of stress and deformation. Furthermore, the numerical values of the parameters (material constants) in the constitutive relationship should be readily derivable from meaningful laboratory test data. The constitutive relationship will serve two purposes: (a) it provides a means for the interpretation and organization of laboratory test data for various

states of stress and deformation, and (b) it can be utilized, in conjunction with the field equations, to perform effective stress analysis for dams, or other earth structures, when subjected to different transient or static-type boundary loading conditions. Once a calculation scheme for effective stress analysis has been established, the potential for liquefaction can be assessed by examining the stress-strain-pore pressure distribution within the earth structure of interest. It should be pointed out that within the framework of this type of analysis, it is the process that leads to liquefaction which is predicted rather than the actual flow of the liquefied material.

3. As part of requirements previously mentioned, a constitutive relationship for saturated sand must be able to treat a two-phase material consisting of solid particles and pore fluid. Within the framework of the theory of continuous mass media, which is the basis for all stress and deformation analyses, there are, in principle, two approaches which can be taken to formulate a constitutive equation for a two-phase system. The first approach is based on the continuum theory of mixtures.[6] The second approach, which may be referred to as a "pseudo mixture theory," is based on the elastic-plastic theory of solids.[7] In this approach, a two-phase system is simulated by simply limiting the overall compressibility of the material to that of the pore fluid and solid particles when drainage is not allowed. The continuum theory of mixtures in the first approach is quite complicated in its full generality. A simplified version of the mixture theory has been applied to solution of liquefaction problems in saturated sand.[8] However, because of the assumption that the solid skeleton of the material is elastic, the theory could not predict progressive increase of pore pressure under cyclic loading conditions.[9] The elastic-plastic constitutive relations are generally based on physical observation of material behavior under laboratory conditions, and have been used successfully for the solution of a number of geotechnical problems.[10,11] They are not mathematically too constrained and one could easily incorporate any physically reasonable material behavior, at least in an ad hoc manner, in their formulation.

Objective

4. The overall objective of the analytical studies of the liquefaction and deformation problem of saturated sands is to develop a rational calculation framework for performing effective stress analyses in realistically posed boundary-value problems. As was pointed out previously, once such a calculational framework has been established, the potential for liquefaction under a specified boundary loading condition can be assessed. The investigation is to be carried out in three phases:

a. Phase I. The first phase of the investigation will be devoted to formulation of a three-dimensional elastic-plastic isotropic constitutive model for saturated sand. During this phase attempts will be made to incorporate in the model some of the basic laboratory observed stress-strain-pore pressure behavior of saturated sand. The constitutive model will then be examined in light of laboratory test data pertinent to the liquefaction phenomenon, at least qualitatively, such as undrained triaxial test results, and any shortcomings of the model will be delineated.

b. Phase II. During the second phase of the investigation the constitutive model will be extended, if necessary, so that it can "successfully" simulate laboratory behavior of saturated sand pertinent to the liquefaction problem.

c. Phase III. During this phase, efforts will be made to incorporate the constitutive model into a suitable numerical computer code for subsequent use in conducting effective stress analysis (and assessing liquefaction potential) under various boundary loading conditions.

The objective of this report is to document the results of Phase I of the investigation.

Scope

5. The development of the constitutive model is presented in Part II. The behavior of the model under axisymmetric triaxial test condition is demonstrated in Part III. Part IV contains the results of comparison of model prediction with laboratory behavior. Conclusions and recommendations are given in Part V. Appendix A contains the fundamental basis of elastic-plastic constitutive models and is included for reference purposes and future use.

PART II: DEVELOPMENT OF CONSTITUTIVE MODEL

Mechanical Behavior of Cohesionless Soil

6. The mechanical response of a cohesionless soil when subjected to externally applied loads is a function of the volumetric and deviatoric stress-strain properties of the material. The stress-strain properties are, in turn, affected by such factors as void ratio, degree of saturation, interstitial pore fluid, and the loading history of the material. Void ratio, in particular, reflects the state of compaction of the material, e.g., loose and dense. Loose sand compacts and exhibits a ductile-type stress-strain behavior when subjected to a deviatoric state of stress. Dense sand, on the other hand, dilates and exhibits a brittle-type stress-strain behavior when subjected to a similar stress condition. The boundary between the loose and dense states is characterized by the void ratio at which shearing deformation occurs without volume change. This void ratio is referred to as "critical void ratio" and its magnitude varies inversely with mean normal stress.[7] This basic difference in the physical behavior of loose and dense sand seems to exist only at relatively low confining pressures. At very high confining pressures (i.e., at confining pressures above the preconsolidation pressure) the shearing stress-strain behavior of dense sand also resembles a ductile-type behavior and is accompanied by compaction. Therefore, the stress-strain behavior of sand is highly dependent on the confining pressure or the superimposed hydrostatic state of stress.

7. The stress-strain behavior of saturated sand also varies greatly depending on whether sand is in the drained or undrained state during loading. Since the pore fluid is relatively incompressible, in the undrained condition pressure builds up in the pore fluid. The effective stress carried by the soil particles is the total stress minus the pore pressure. It is, therefore, the effective confining pressure that influences the stress-strain behavior of saturated sand.

8. In summary, the stress-strain behavior of a saturated sand depends on its initial void ratio, the current and past loading history,

and the effective confining pressure. Yield and deformation in the undrained condition typically resemble the characteristics shown in Figure 1. In the next section, the development of an elastic-plastic constitutive relationship that partially describes the behavior shown in Figure 1 is presented.

Constitutive Model

9. The fundamental basis of elastic-plastic constitutive models is presented in Appendix A. The elastic behavior of the models is defined by Equations A11 through A16 of Appendix A. The plastic behavior of the models is described by Equations A17 through A28. The complete elastic-plastic description is governed by Equations A29 and A30. To apply these equations to a two-phase continuum, consisting of solid skeleton and pore fluid, the normal stress components should be divided into two parts; the stress carried by the solid structure, referred to as effective stress, and the stress carried by pore fluid, referred to as pore water pressure. Mathematically, total stress can be expressed as

$$\sigma = \sigma' + u \tag{1a}$$

or, in tensorial form, as

$$\sigma_{ij} = \sigma'_{ij} + u\,\delta_{ij} \tag{1b}$$

where

σ_{ij} = total stress tensor

σ'_{ij} = effective stress tensor

δ_{ij} = Kronecker delta

For example, in the case of triaxial test in cylindrical coordinate system z , r , and θ , Equation 1 takes the following form

$$\left.\begin{aligned} \sigma_z &= \sigma'_z + u \\ \sigma_\theta = \sigma_r &= \sigma'_r + u = \sigma'_\theta + u \end{aligned}\right\} \tag{2}$$

where σ_z and $\sigma_r = \sigma_\theta$ are, respectively, the axial and radial stress components. The mathematical forms of various response functions for the proposed constitutive relationship for saturated sand are presented in the following paragraphs.

10. For the elastic (recoverable) response of the material it is assumed that the bulk modulus K is a linear function of pressure; thus,

$$K = K_i + K_1 J_1'/3 = K_i + K_1 P' \tag{3}$$

where K_i and K_1 are material constants which can be determined from the slope of the unloading curve from an isotropic consolidation test (Figure 2). The quantity J_1' is the first invariant of stress tensor and P' is the effective mean normal stress ($P' = \frac{\sigma_z' + 2\sigma_r'}{3}$ for triaxial test). The elastic shear modulus G is assumed to be constant (in general the shear modulus is a function of the state of stress and strain. For simplicity and as a first order of approximation, however, it is assumed to be constant).

11. For the plastic behavior the loading function f (Equation A9) is assumed to be isotropic and to consist of two parts (Figure 3): an ultimate failure envelope which serves to limit the maximum shear strength of the material

$$f\left(\sqrt{\bar{J}_2}, J_1'\right) = \sqrt{\bar{J}_2} - \frac{M}{3\sqrt{3}} J_1' \tag{4}$$

and a strain-hardening cap

$$F\left(\sqrt{\bar{J}_2}, J_1', \kappa\right) = (J_1' - L)^2 + R^2 \bar{J}_2 - (X - L)^2 \tag{5}$$

The quantity $\sqrt{\bar{J}_2}$ is the second invariant of stress deviation tensor ($\bar{J}_2 = (\sigma_z' - \sigma_r')^2/3$ for triaxial test). The hardening function κ which controls material compaction and/or dilatation is assumed to be equal to the plastic volumetric strain (ε_{kk}^P) and takes the following form

$$\kappa = \varepsilon_{kk}^{P} = \frac{1}{K_2} \ln \left(\frac{K_2}{K_0}\frac{X}{3} + 1\right) - \frac{1}{K_1} \ln \left(\frac{K_1}{K_i}\frac{X}{3} + 1\right) \qquad (6)$$

The intersection of the cap with the J_1' axis is denoted by X. The ratio of the major to the minor axis of the elliptic cap is denoted by R. The value of J_1' at the center of the cap is denoted by L which is related to other parameters by the relation

$$L = \frac{X}{1 + \frac{RM}{3\sqrt{3}}} \qquad (7)$$

Equation 7 indicates that the failure envelope (Equation 4) intersects each ellipse at the crown.

12. The material constants K_0 and K_2 in Equation 6 are determined from the slope of the loading curve from an isotropic consolidation test (Figure 2). The conditions of uniqueness and stability have to be satisfied in determining the material constants K_i, K_1, K_0, and K_2. These conditions are satisfied if the following inequalities are adhered to:

$$K_i \geq K_0 \qquad (8a)$$

$$K_1 \geq K_2 \qquad (8b)$$

The parameter M (Equation 4) is indicative of the frictional strength of the material and is related to the effective angle of internal friction ϕ' through the following relation (for triaxial compression)

$$M = \frac{6 \sin \phi'}{3 - \sin \phi'} \qquad (9)$$

13. In summary, there are seven material constants that describe the behavior of the proposed model, i.e., K_i, K_1, K_0, K_2, G, M, and R. A more complicated (and possibly more realistic) model can be developed by replacing these constants with appropriate mathematical expressions that are functions of stress and/or strain invariants.

14. It should be noted that the proposed model allows for the elliptic caps to expand as well as to translate relative to the origin of

the J_1' , $\sqrt{J_2}$ axis. Thus, the model incorporates both isotropic and some form of kinematic hardening. In the special case where $X = 2L$, i.e., $R = \frac{3\sqrt{3}}{M}$, the strain-hardening cap is not allowed to translate and only expands isotropically. In this case, the number of material constants reduces to six and the plastic behavior of the model becomes similar to the model proposed by Schofield and Wroth.[7] In the present model, however, only a portion of the elliptic cap is used as loading function, i.e.,

$$f = \begin{cases} f\left(\sqrt{J_2}\ ,\ J_1'\right) . & \text{if } L \geq J_1' \\ \\ F\left(\sqrt{J_2}\ ,\ J_1'\ ,\ \varepsilon_{kk}^P\right) & \text{if } L < J_1' \end{cases} \tag{10}$$

Schofield and Wroth, on the other hand, use the entire cap as loading function. It is believed that the use of the entire cap violates the Drucker[12] stability postulate which is sufficient, although not necessary, to satisfy all thermodynamic and continuity requirements of the incremental theory of plasticity. Stability ensures that all physically reasonable initial-boundary-value problems are properly posed in the mathematical sense.

15. An undrained condition is simulated by the model by imposing the condition

$$d\varepsilon_{kk} = 0 \tag{11}$$

where $d\varepsilon_{kk}$ is the increment of total volumetric strain. The model then calculates the stress path (and the associated material response) corresponding to Equation 11. This stress path is assumed to be the effective stress path that the material will experience during an undrained test. Within the framework of elastic-plastic models (Appendix A) Equation 11 can be satisfied by allowing the increment of plastic volumetric strain ($d\varepsilon_{kk}^P$) to be the negative of the increment of elastic volumetric

strain ($d\varepsilon_{kk}^{E}$) . For the drained condition the model simply calculates the response of the material (including volumetric strain) for any specified stress path. The response of the material under axisymmetric triaxial test condition is demonstrated in Part III.

PART III: BEHAVIOR OF THE CONSTITUTIVE MODEL IN AN AXISYMMETRIC TRIAXIAL TEST CONDITION

16. Most of the mechanical testing of sand for engineering purposes is performed in the triaxial test apparatus. It is of interest, therefore, to investigate the behavior of the proposed model in a triaxial test under both drained and undrained conditions. Adopting the z-axis of a cylindrical coordinate system (z , r , and θ) as the axis of symmetry of the soil sample, the effective stress tensor and strain tensor associated with the triaxial test become ($\sigma'_\theta = \sigma'_r$ and $\varepsilon_\theta = \varepsilon_r$)

$$\sigma'_{ij} = \begin{bmatrix} \sigma'_z & 0 & 0 \\ 0 & \sigma'_r & 0 \\ 0 & 0 & \sigma'_r \end{bmatrix} \tag{12a}$$

$$\varepsilon_{ij} = \begin{bmatrix} \varepsilon_z & 0 & 0 \\ 0 & \varepsilon_r & 0 \\ 0 & 0 & \varepsilon_r \end{bmatrix} \tag{12b}$$

The variables $P' = J'_1/3$ (effective mean normal stress), $\bar{J}_2$ (the second invariant of stress deviation tensor), and $\varepsilon_{kk}/3$ (mean volumetric strain) associated with the above stress and strain tensors take the following forms

$$P' = J'_1/3 = \frac{\sigma'_z + 2\sigma'_r}{3} \tag{13a}$$

$$\bar{J}_2 = \frac{1}{3}\ (\sigma'_z - \sigma'_r)^2 \tag{13b}$$

$$\frac{1}{3}\frac{\Delta V}{V} = \frac{\varepsilon_{kk}}{3} = \frac{\varepsilon_z + 2\varepsilon_r}{3} \tag{13c}$$

Isotropic Consolidation Phase

17. During isotropic consolidation phase of the triaxial test

$$\sigma_z' = \sigma_r' = J_1'/3 = P' \tag{14a}$$

$$\varepsilon_z = \varepsilon_r = \frac{\varepsilon_{kk}}{3} \tag{14b}$$

The relation between the elastic volumetric strain increment and the increment of effective mean normal stress is given as (see Equation A12)

$$dP' = K\, d\varepsilon^E_{kk} \tag{15}$$

where the elastic bulk modulus K is given in Equation 3. Substituting Equation 3 in Equation 15 and integrating the resulting expression provides the following relation between the elastic volumetric strain ε^E_{kk} and pressure

$$\varepsilon^E_{kk} = \frac{1}{K_1} \ln \left(\frac{K_1}{K_i} P' + 1 \right) \tag{16}$$

The relation between the plastic volumetric strain ε^P_{kk} and pressure is given in Equation 6. During isotropic consolidation $\frac{X}{3}$ in Equation 6 should be replaced by P', thus

$$\varepsilon^P_{kk} = \frac{1}{K_2} \ln \left(\frac{K_2}{K_0} P' + 1 \right) - \frac{1}{K_1} \ln \left(\frac{K_1}{K_i} P' + 1 \right) \tag{17}$$

In view of Equations 16 and 17 the total volumetric strain takes the following form

$$\varepsilon_{kk} = \frac{1}{K_2} \ln \left(\frac{K_2}{K_0} P' + 1 \right) \tag{18}$$

Equations 16 through 18 provide a complete specification for the behavior of the material during isotropic consolidation test.

18. The qualitative behavior of the model during isotropic consolidation is shown in Figure 4. The slope of the pressure-volumetric strain curve during virgin loading can be obtained from Equation 18

$$\frac{dP'}{d\varepsilon_{kk}} = K_2 P' + K_0 = \tilde{K} \tag{19}$$

Combining Equations 19 and 17 results in

$$\tilde{K} = \frac{K_1 P' + K_i}{1 + (K_1 P' + K_i) \dfrac{d\varepsilon_{kk}^P}{dP'}} = \frac{K}{1 + K \dfrac{d\varepsilon_{kk}^P}{dP'}} \tag{20}$$

The second term in the denominator of Equation 20 produces an apparent softening of the modulus $\tilde{K}$ due to plastic compaction. For a very dense sand, the softening term is very small, and the modulus $\tilde{K}$ approaches the elastic bulk modulus K. Also, if a sample is consolidated from point 1 to point 2 (Figure 4), unloaded from point 2 to point 3, and then reloaded from point 3 to point 2, the model dictates that the reloading behavior is purely elastic and the second term in the denominator of Equation 20 is zero. This type of behavior, however, may not be completely true for an actual sand and is only a mathematical idealization.

Shear Phase

19. During the shear phase of a conventional triaxial test cell pressure is constant

$$\sigma_r = \text{constant} = P_c \tag{21a}$$

$$d\sigma_r = 0 \tag{21b}$$

where P_c is the confining pressure at the end of the isotropic consolidation phase. For an undrained test the volumetric strain is constant

during the shear phase and is equal to the volumetric strain achieved at the end of the consolidation phase of the test. Accordingly, for an undrained test

$$d\varepsilon_{kk} = d\varepsilon^{E}_{kk} + d\varepsilon^{P}_{kk} = 0 \tag{22a}$$

which leads to

$$d\varepsilon_{r} = -\frac{1}{2} d\varepsilon_{z} \tag{22b}$$

The plastic volumetric strain, or the hardening function, during the shear phase is given by Equation 6. In view of Equations 16 and 6, the total volumetric strain becomes

$$\varepsilon_{kk} = \frac{1}{K_1} \ell n \left(\frac{K_1}{K_i} P' + 1\right) + \frac{1}{K_2} \ell n \left(\frac{K_2}{K_0} \frac{X}{3} + 1\right)$$

$$- \frac{1}{K_1} \ell n \left(\frac{K_1}{K_i} \frac{X}{3} + 1\right) \tag{23}$$

For the undrained condition, since ε_{kk} is constant and is equal to the volumetric strain achieved at the end of the isotropic consolidation phase (Equation 18), Equation 23 becomes

$$\varepsilon_{kk}\Big|_{P = P_c} = \frac{1}{K_2} \ell n \left(\frac{K_2}{K_0} P_c + 1\right) = \text{constant}$$

$$= \frac{1}{K_1} \ell n \left(\frac{K_1}{K_i} P' + 1\right) + \frac{1}{K_2} \ell n \left(\frac{K_2}{K_0} \frac{X}{3} + 1\right) - \frac{1}{K_1} \ell n \left(\frac{K_1}{K_i} \frac{X}{3} + 1\right) \tag{24}$$

The equation of the elliptic cap (Equation 5) for triaxial configuration takes the following form

$$(P' - \frac{L}{3})^2 + \frac{R^2}{27} (\sigma'_z - \sigma'_r)^2 - (\frac{X}{3} - \frac{L}{3})^2 = 0 \tag{25}$$

Equations 24 and 25 can be combined to determine an expression for the effective stress path (i.e., $\sigma_z' - \sigma_r'$ versus P') for the undrained condition. Having determined the effective stress path the pore water pressure can be obtained from Equation 1. The total strain can be obtained from Equation A29. A computer program, called TDRIVER, was developed to numerically solve the above system of equations and generate various plots of stress-strain-pore pressure response for undrained conditions. This program and its flow charts are available upon request. Typical results from computer code TDRIVER are presented in Part IV. Figure 5 depicts qualitatively the effect of the parameter R on the stress-strain-pore pressure response for conventional triaxial test. It is noted from Figure 5 that R has a substantial influence on the behavior of the model (the value of R reflects the relative density of the material, i.e., the denser the material the smaller the value of R).

20. In the case of drained test the response of the material, for a given stress path, is determined from Equations 23, 25, and A29. Typical results for drained condition predicted by the model are shown qualitatively in Figure 6.

PART IV: COMPARISON OF LABORATORY TEST DATA WITH MODEL PREDICTION

Experimental Program

21. The experimental program consisted of two series of tests conducted on saturated samples of Reid Bedford Model sand. The gradation curve for the Reid Bedford Model sand is shown in Figure 7. The material consists of subround to subangular particles. Each test series consisted of a load/unload isotropic consolidation test and four conventional consolidated undrained triaxial tests. Saturation of the specimens was achieved by backpressure saturation. The first test series was conducted on specimens having a relative density of approximately 76 percent. Relative density for the second series of tests was about 38 percent. Test data from the first series of tests are documented in Plates 1 through 3. Plate 1 depicts the results of the isotropic consolidation test presented in terms of a plot of effective mean normal stress versus volumetric strain. The results of the triaxial tests are shown in Plates 2 and 3 in terms of principal stress difference and excess pore pressure versus axial strain, respectively. The corresponding results from the second test series are documented in Plates 4 through 6.

Material Constants

22. As was pointed out previously, there are seven material constants associated with the proposed constitutive model which must be determined experimentally. Four of the material constants (K_i , K_1 , K_0 , and K_2) are associated with the isotropic consolidation test (see Figure 2). The parameter M is the slope of the ultimate failure envelope of the material plotted in the principal stress difference-effective mean normal stress space (see Figure 3). The elastic shear modulus G (assumed to be a constant in the proposed model) can be estimated from unloading slopes of principal stress difference-principal strain difference plots. The parameter R (the ratio of the major to the minor axis of the elliptic cap) can be determined directly from K_o test results. For this study, however, since K_o test results were not available, the value of

the parameter R was selected in order to obtain a good fit to the experimental effective stress paths. The value of shear modulus was selected to obtain a reasonable fit to experimental stress-strain curves. The final values of the material constants for the two test series are given in Table 1.

Comparison of Test Results with Model Behavior

23. Figures 8 through 10 depict comparison plots of test results with model behavior for the first test series (relative density 76 percent) for consolidation pressures of 0.72 and 7.2 tsf. Figure 8 shows plots of effective stress paths in the principal stress difference-effective mean normal stress space. Principal stress difference versus axial strain relations are shown in Figure 9. Figure 10 depicts plots of excess pore pressure versus axial strain relations. The corresponding set of plots for the second test series (relative density 38 percent) is presented in Figures 11 through 13. For the purpose of model calculations the yield function F (the elliptic cap) was used as loading function from the beginning of the test until the effective stress path reached the ultimate failure envelope f . From then on, the ultimate failure envelope was used as loading function. During the first part of the calculation (i.e., using F as loading function) excess pore pressure increased and reached its maximum value when the effective stress path reached the ultimate failure envelope. From then on, excess pore pressure decreased and eventually became negative as the test continued. As observed from Figures 8 through 13, the proposed constitutive model qualitatively simulates the stress-strain-pore pressure response of the material for both test series.

24. In order to evaluate the effect of the parameter R on the stress-strain-pore pressure response of the material and to show the capability of the model in simulating the behavior of loose sand, three calculations were performed for a hypothetical material having properties K_i = 70 tsf , K_1 = 37 , K_0 = 40 tsf , K_2 = 3.7 , M = 1.02 , and G = 50 tsf. The results of the calculations are presented in Figure 14 for three different values of R . The curves marked B are associated with a

base line value of $R = R_B = 5.09$. This value of R corresponds to $\frac{3\sqrt{3}}{M}$ which, as was pointed out previously, allows for the strain-hardening cap to expand isotropically only. The curves marked A and C are associated with R values of $4R_B$ and $R_B/4$, respectively. It is noted from Figure 14 that the parameter R significantly controls the stress-strain-pore pressure response of the material.* In general, for a given confining pressure, the greater the value of R the smaller the shear strength of the material and the larger the induced pore pressure. For a given confining pressure, smaller values of R are associated with higher shear strengths and lower pore pressures.

---

* For the hypothetical material the calculations were terminated when the effective stress path reached the ultimate failure envelope f .

PART V: CONCLUSIONS AND RECOMMENDATIONS

25. A three-dimensional elastic-plastic isotropic constitutive relationship has been developed that qualitatively simulates certain characteristics of the stress-strain-pore pressure response of saturated granular materials. In particular, the constitutive relationship accounts for the hysteretic behavior of pressure-volumetric strain response of sand, the effect of superimposed hydrostatic stress on shearing response, and the shear-induced volume change.

26. The constitutive equation does not treat work-softening behavior (Figure 1, curve No. 2), and can not predict a progressive increase of pore pressure under low-amplitude (subyield) cyclic loading conditions. Both of these phenomena are important features which contribute to liquefaction of saturated sand.

27. It is recommended that during the second phase of this investigation the present constitutive equation be extended to account for the strain-softening behavior and the progressive increase of pore pressure observed under cyclic loading conditions. This extension is a major task from a theoretical point of view, but can be accomplished within the basic structure of the present model. Preliminary investigations have indicated that such an extension may be accomplished in a number of ways. It may be necessary to try several techniques and adopt the one which best simulates the experimental data while at the same time satisfying all theoretical requirements. However, as a basic requirement to any feasible technique the compressibility of pore fluid and soil skeleton must be included in the analysis of undrained behavior.

28. If the extension of the present model is successfully accomplished, it is further recommended that during Phase II of this study the shear modulus G and the parameter R (the ratio of the major to the minor axis of the elliptic loading function) be replaced by appropriate functional forms in order to quantitatively, as well as qualitatively, simulate the stress-strain-pore pressure response of saturated granular materials. This modification is a relatively simple task (in comparison

with extension of the model discussed in paragraph 27) from a theoretical point of view. The particular functional forms of G and R, however, must be selected based on experimental observation of material behavior under diverse loading conditions.

REFERENCES

1. Youd, T. L., "Liquefaction, Flow, and Associated Ground Failure," Geological Survey Circular 688, 1973, United States Department of Interior, Washington, D. C.

2. Castro, G., "Liquefaction of Sands," Harvard Soil Mechanics Series No. 81, 1969.

3. Seed, H. B., and Lee, K. L., "Liquefaction of Saturated Sands During Cyclic Loading," Journal, Soil Mechanics and Foundation Division, American Society of Civil Engineers, Vol 92, No. SM6, 1966, pp 105-134.

4. Ishihara, K., Tatsuoka, F., and Yasuda, S., "Undrained Deformation and Liquefaction of Sand Under Cyclic Stresses," Journal, Soils and Foundation, Japanese Society of Soil Mechanics and Foundation Engineering, Vol 15, No. 1, Mar 1975, pp 29-44.

5. Casagrande, A., "Liquefaction and Cyclic Deformation of Sands; A Critical Review," Harvard Soil Mechanics Series No. 88, Cambridge, Massachusetts, Jan 1976, Presented at Fifth Panamerican Conference on Soil Mechanics and Foundation Engineering, Buenos Aires, Argentina, Nov 1975.

6. Passman, S. L., "Mechanics and Thermodynamics of a Mixture of a Granular Material with a Fluid," Mathematics Research Center, MRC Technical Summary Report #1391, University of Wisconsin-Madison, Madison, Wisconsin, Apr 1974.

7. Schofield, A. N. and Wroth, P., "Critical State Soil Mechanics," McGraw-Hill, New York, 1968.

8. Ghaboussi, J. and Wilson, E. L., "Liquefaction Analysis of Saturated Granular Soils," Proceedings, Fifth World Conference on Earthquake Engineering, Rome, 1973.

9. Geoffrey, R. M., Liam Finn, W. D., and Seed, H. B., "Fundamentals of Liquefaction Under Cyclic Loading," Soil Mechanics Series No. 23, University of California, Berkeley, Feb 1974.

10. Baladi, G. Y. and Nelson, I., "Ground Shock Calculation Parameter Study; Report 3, Influence of Type of Constitutive Model on Ground Motion Calculations," Technical Report S-71-4, U. S. Army Engineer Waterways Experiment Station, Vicksburg, Mississippi, April 1974.

11. Nelson, I., Baron, M. L., and Sandler, I., "Mathematical Models for Geological Materials for Wave Propagation Studies," Shock Waves and Mechanical Properties of Solids, Syracuse University Press, 1971, (presented at the 17th Army Material Research Conference, Sep 1970).

12. Drucker, D. C., "On Uniqueness in the Theory of Plasticity," Q. Applied Mathematics, Vol 14, 1956.

13. Handleman, G. H. et al., "On the Mechanical Behavior of Metals in the Strain-Hardening Range," Q. Applied Mathematics, Vol 4, 1947, pp 397-407.

Table 1

Numerical Values of Material Constants

for Reid Bedford Model Sand

Test Series	K_i tsf	K_1	K_0 tsf	K_2	M	G* tsf	R*
1 (relative density ≈ 76%)	90.0	244.0	72.0	160.0	1.53	240.0	0.05
2 (relative density ≈ 38%)	57.5	208.0	36.0	142.0	1.33	100.0	1.5

* Selected to give good fit to experimental data, in lieu of being determined from separate tests.

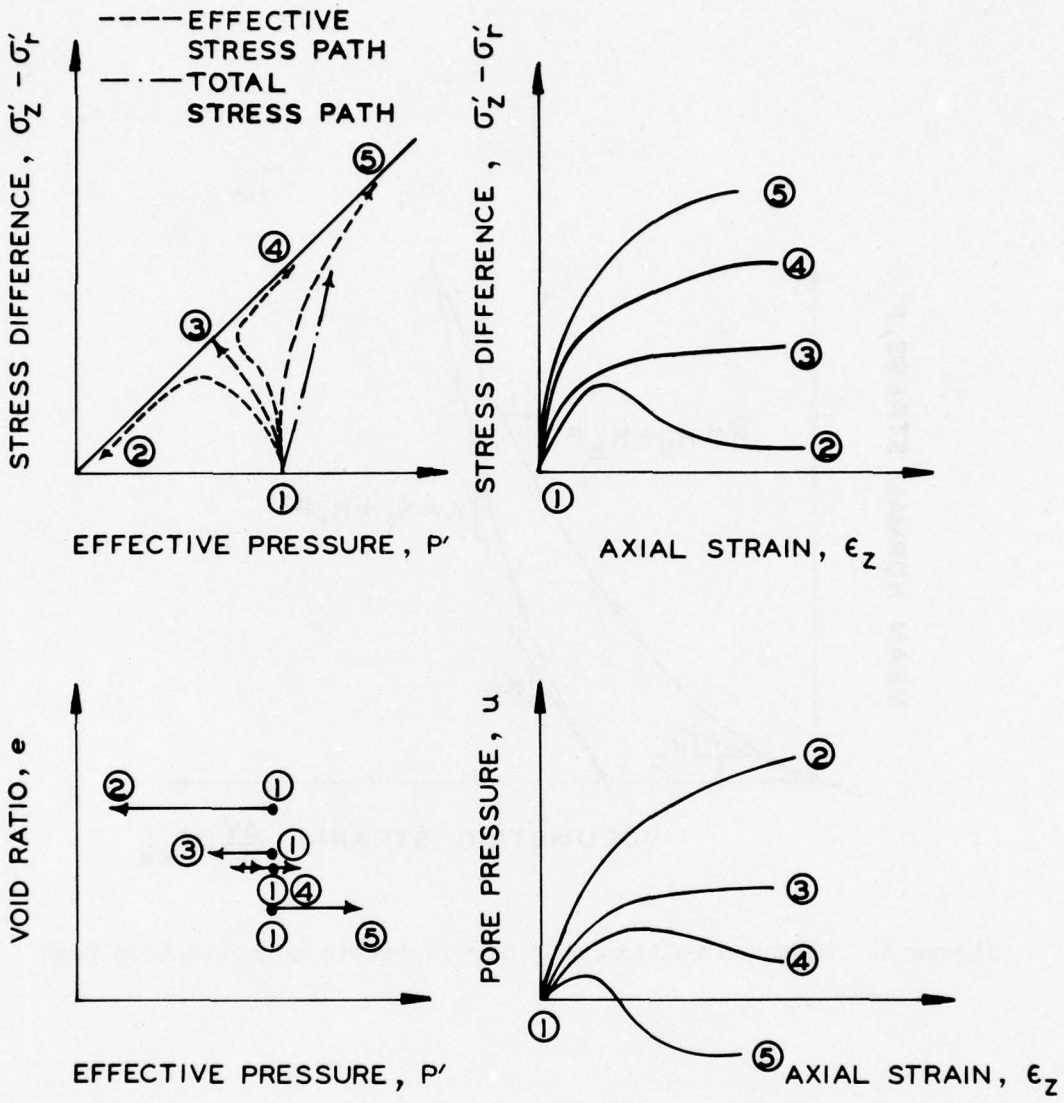

Figure 1. Typical behavior of saturated sand in undrained axisymmetric triaxial test condition

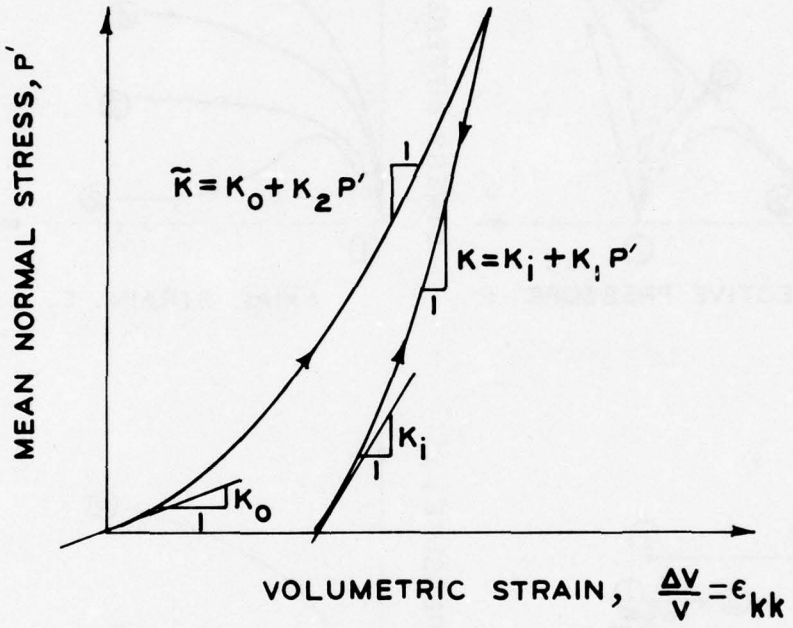

Figure 2. Proposed relationship for isotropic consolidation test

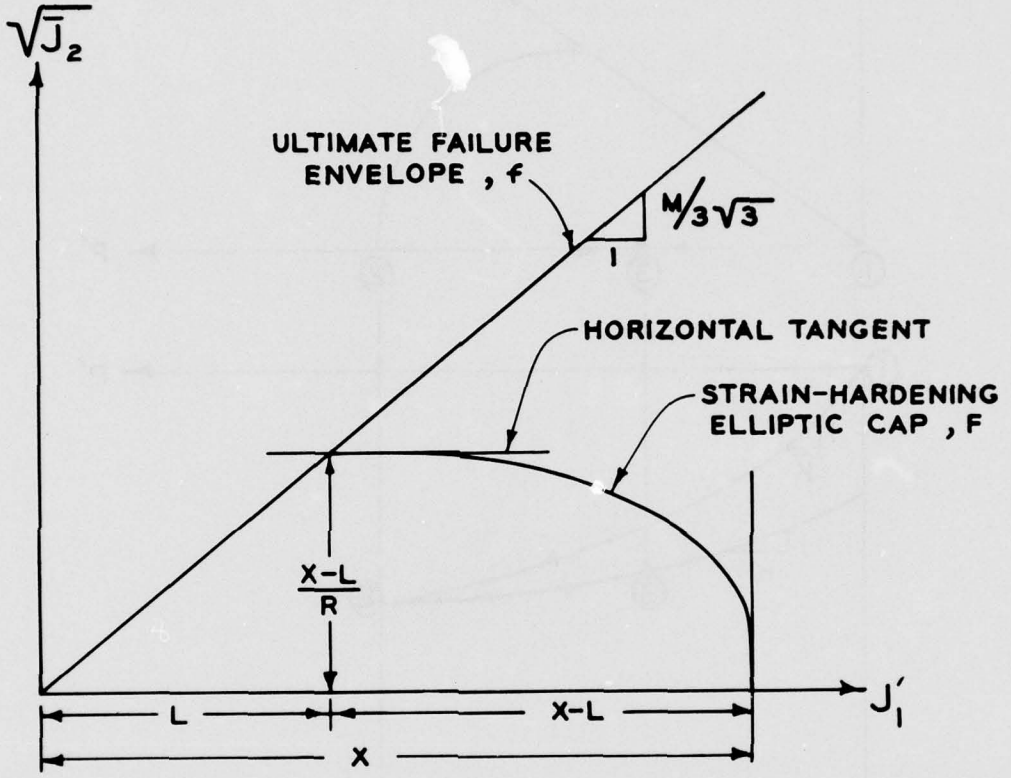

Figure 3. Proposed yield surface for the elastic-plastic model

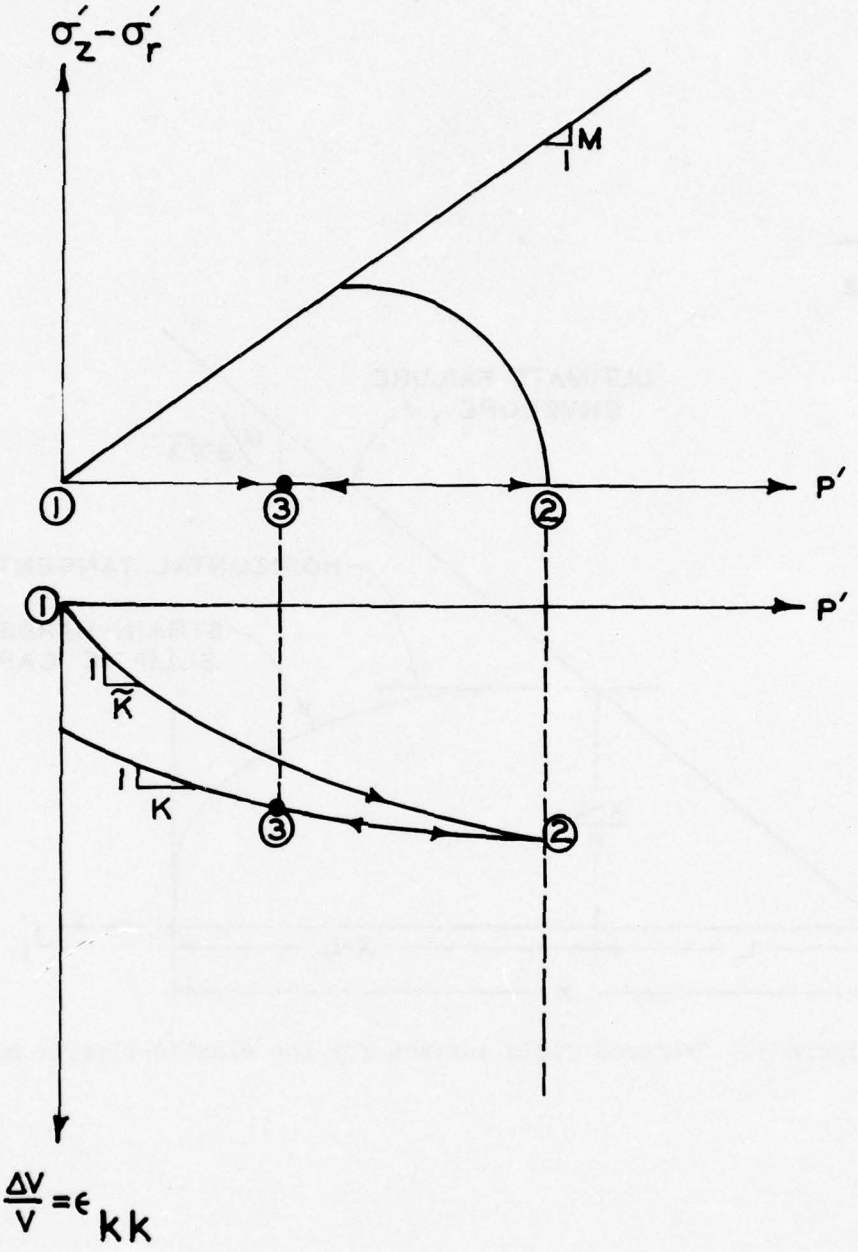

Figure 4. Behavior of the model under isotropic consolidation test

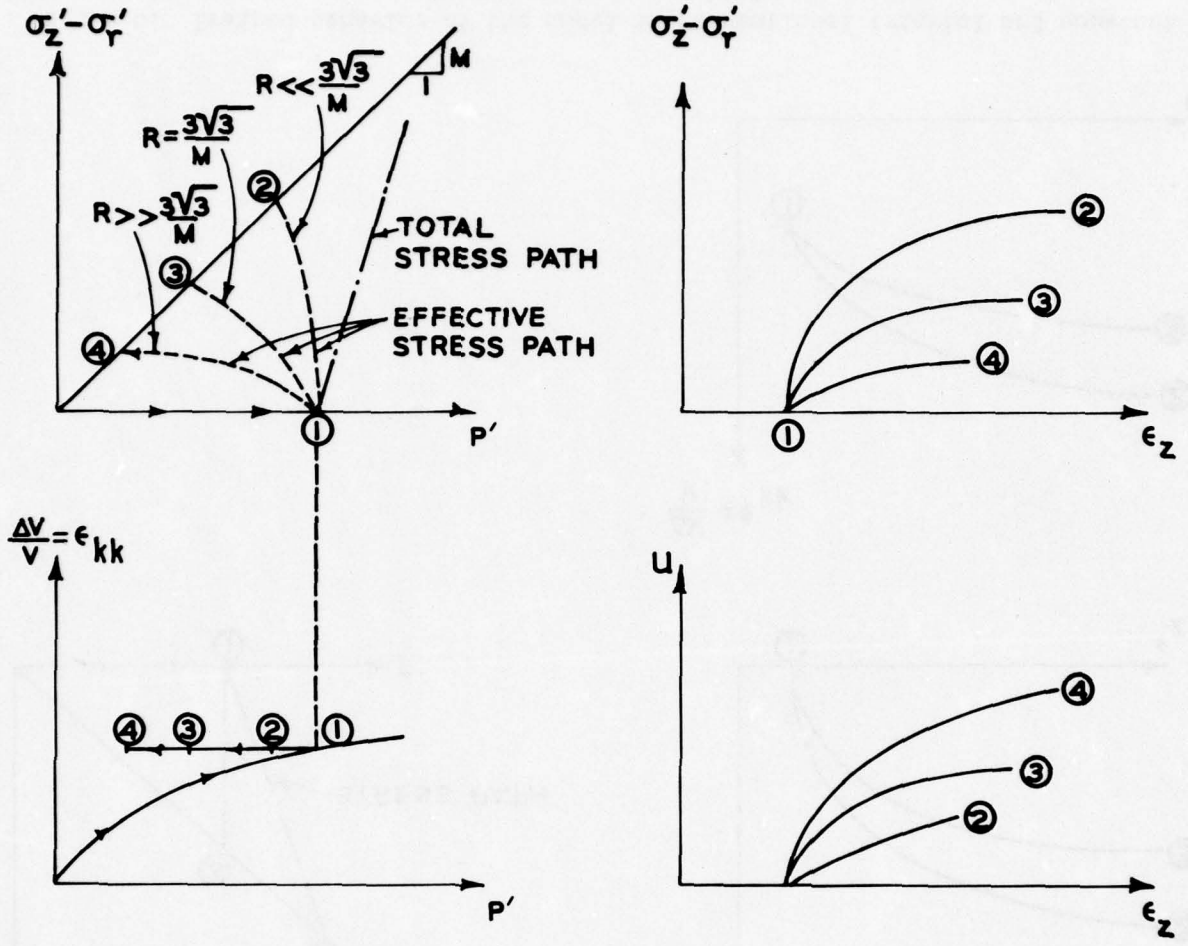

Figure 5. Influence of the parameter R on the behavior of the model for an undrained conventional triaxial test

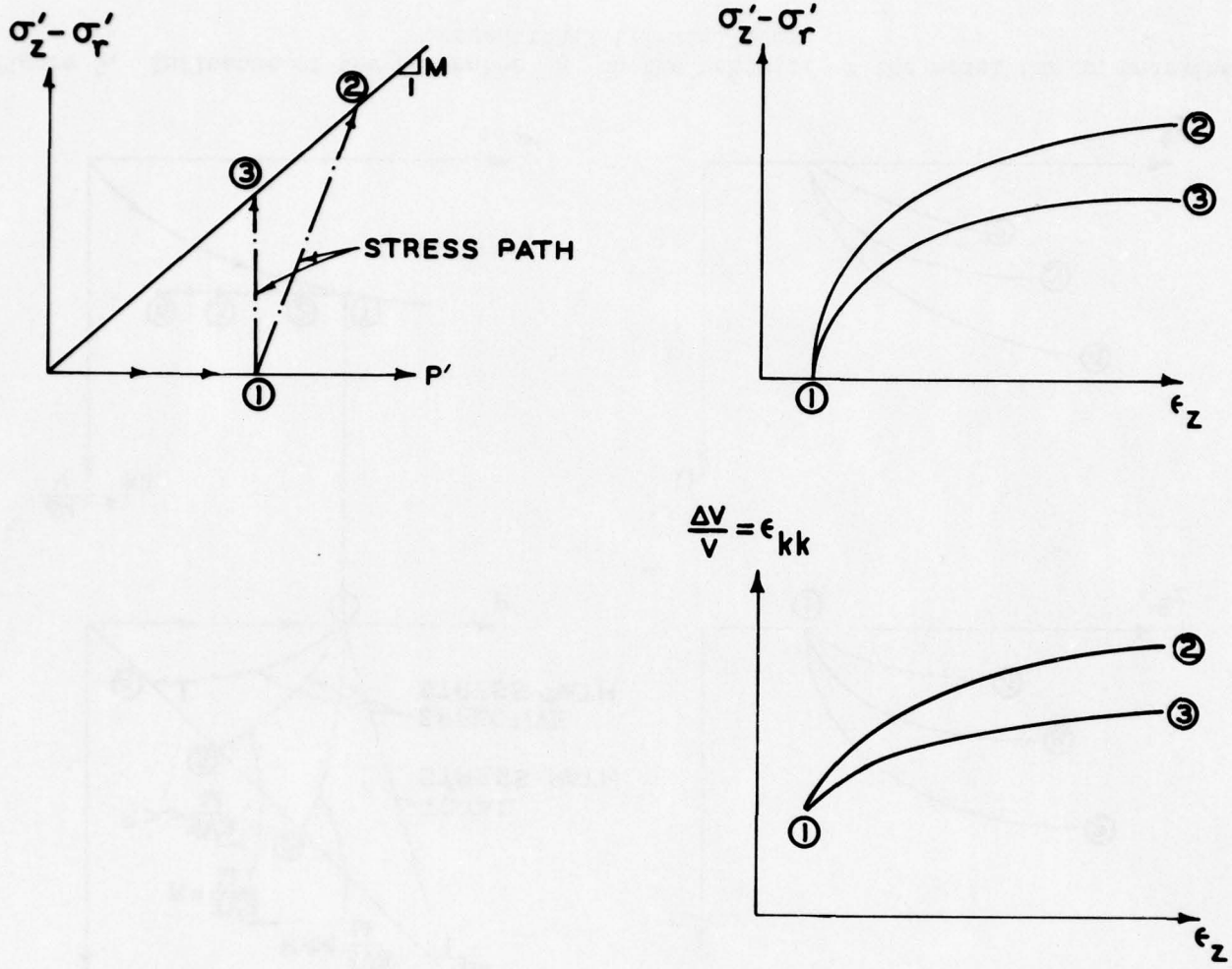

Figure 6. Drained behavior of the model in conventional triaxial and constant mean normal stress tests

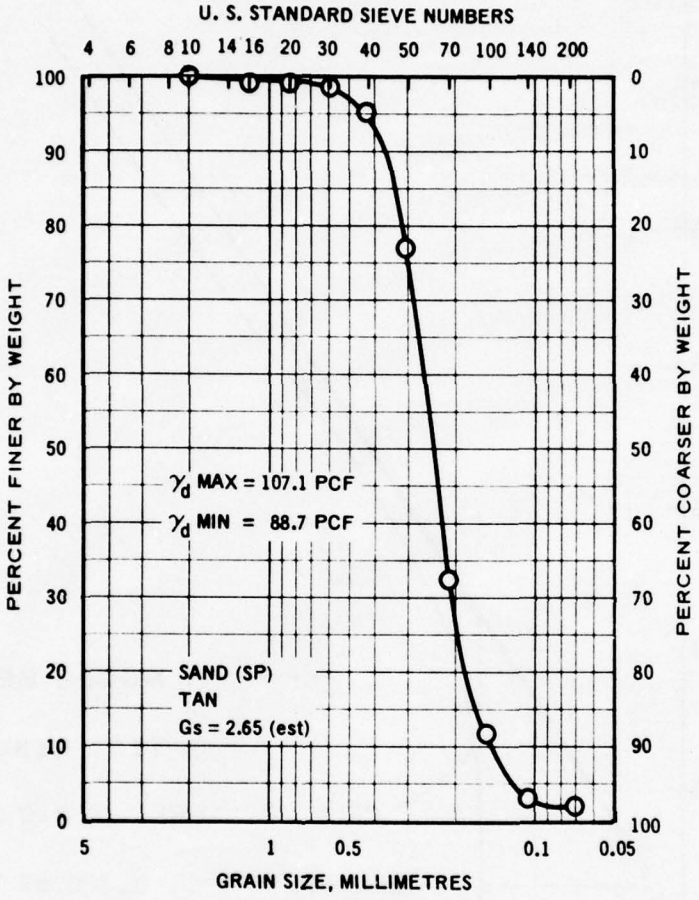

Figure 7. Reid Bedford Model sand grain size distribution curve

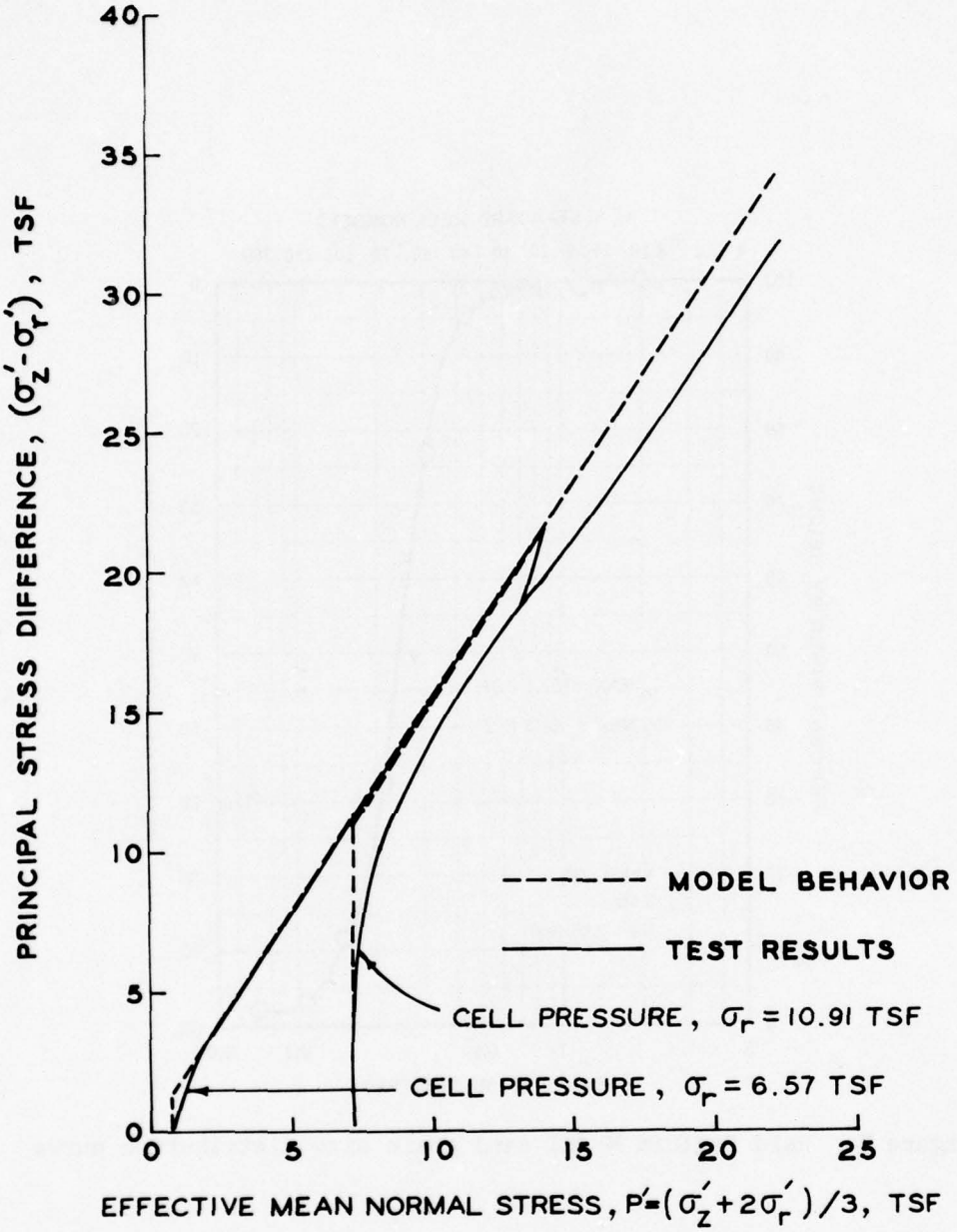

Figure 8. Comparison of effective stress paths produced by the model with test data for saturated Reid Bedford Model sand in undrained triaxial shear (Test Series 1)

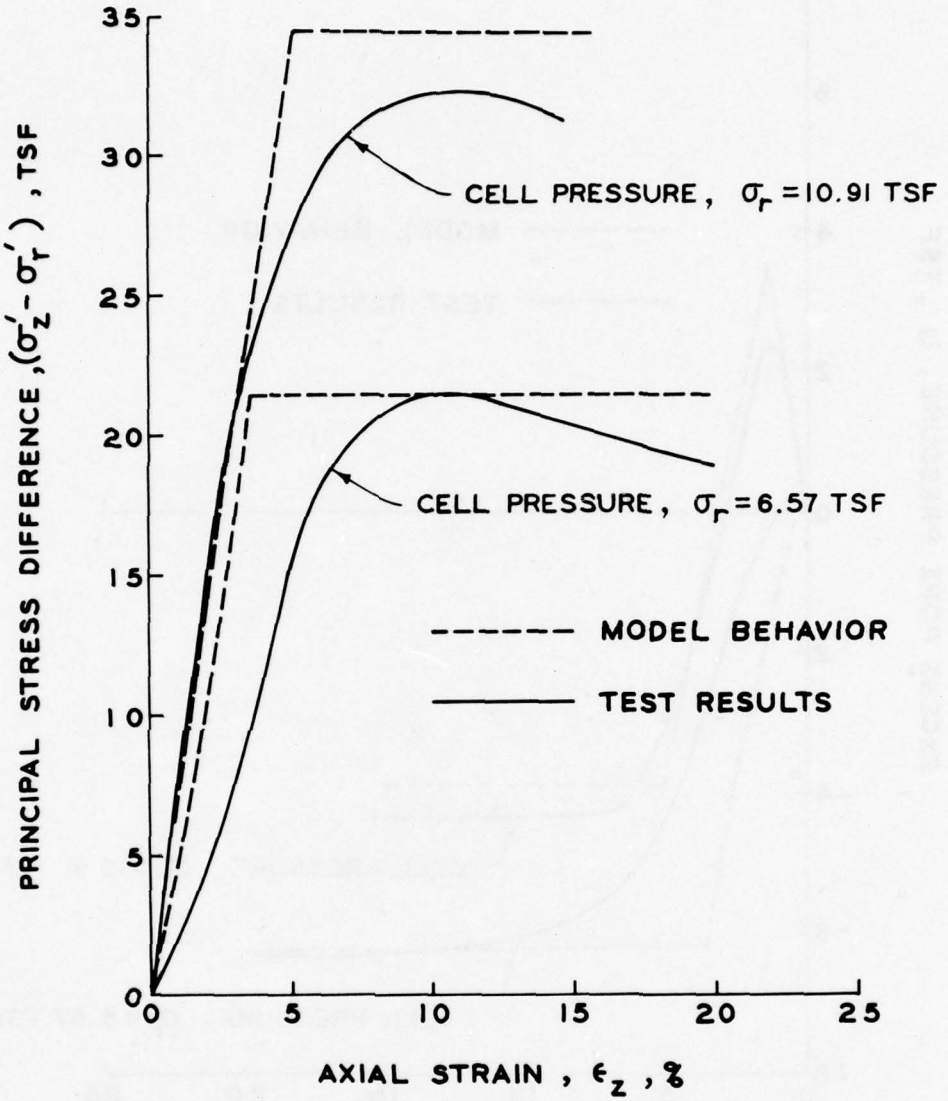

Figure 9. Comparison of principal stress difference vs axial strain relations produced by the model with test data for saturated Reid Bedford Model sand in undrained triaxial shear (Test Series 1)

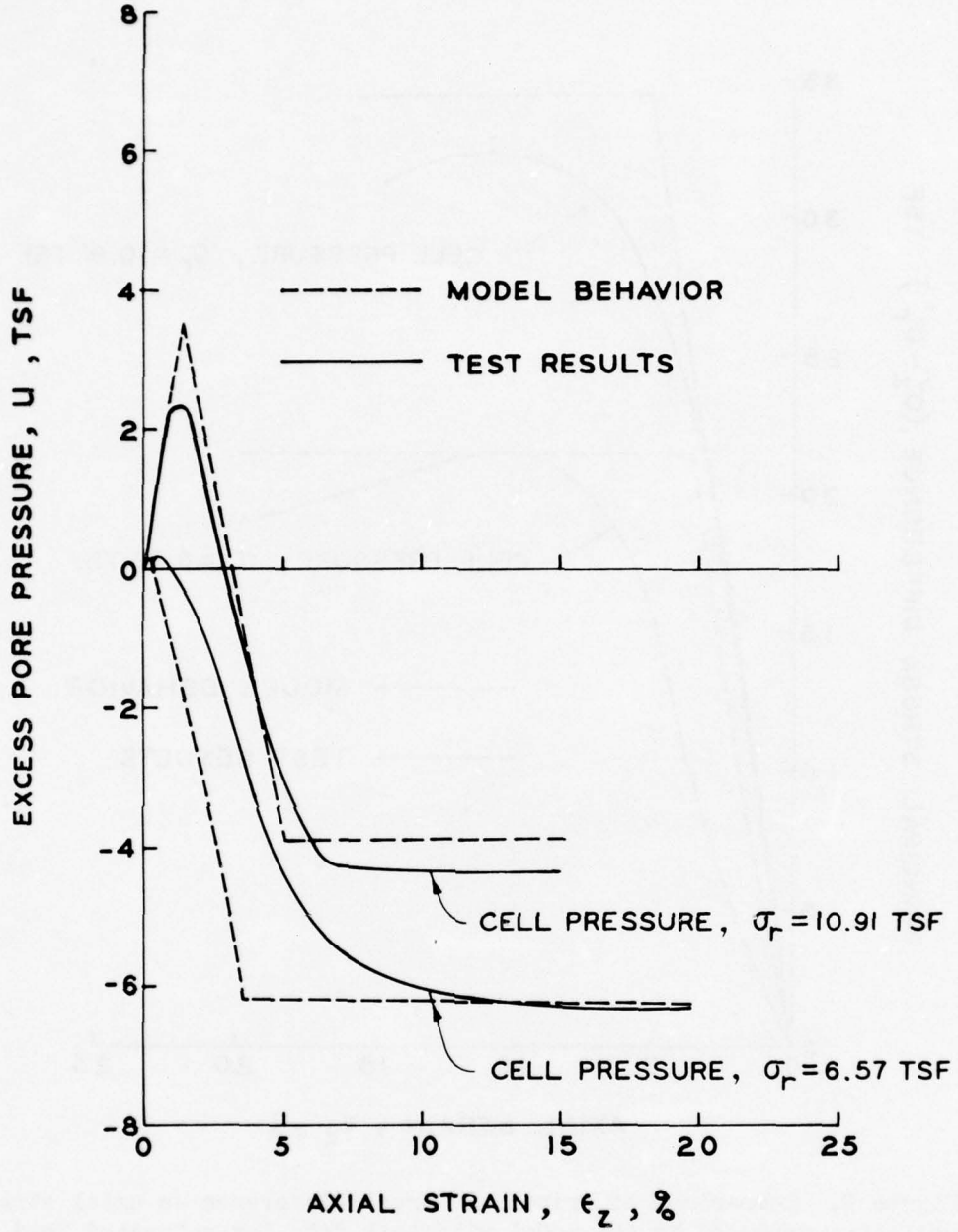

Figure 10. Comparison of excess pore water pressure vs axial strain produced by the model with test data for Reid Bedford Model sand in undrained triaxial shear (Test Series 1)

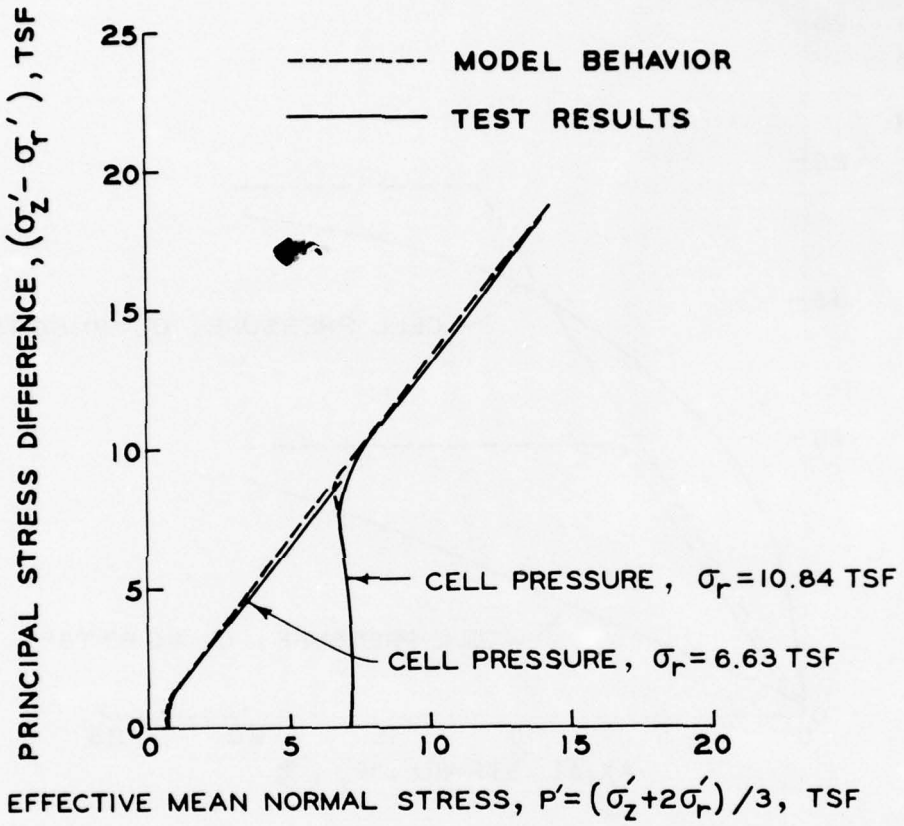

Figure 11. Comparison of effective stress paths produced by the model with test data for saturated Reid Bedford Model sand in undrained triaxial shear (Test Series 2)

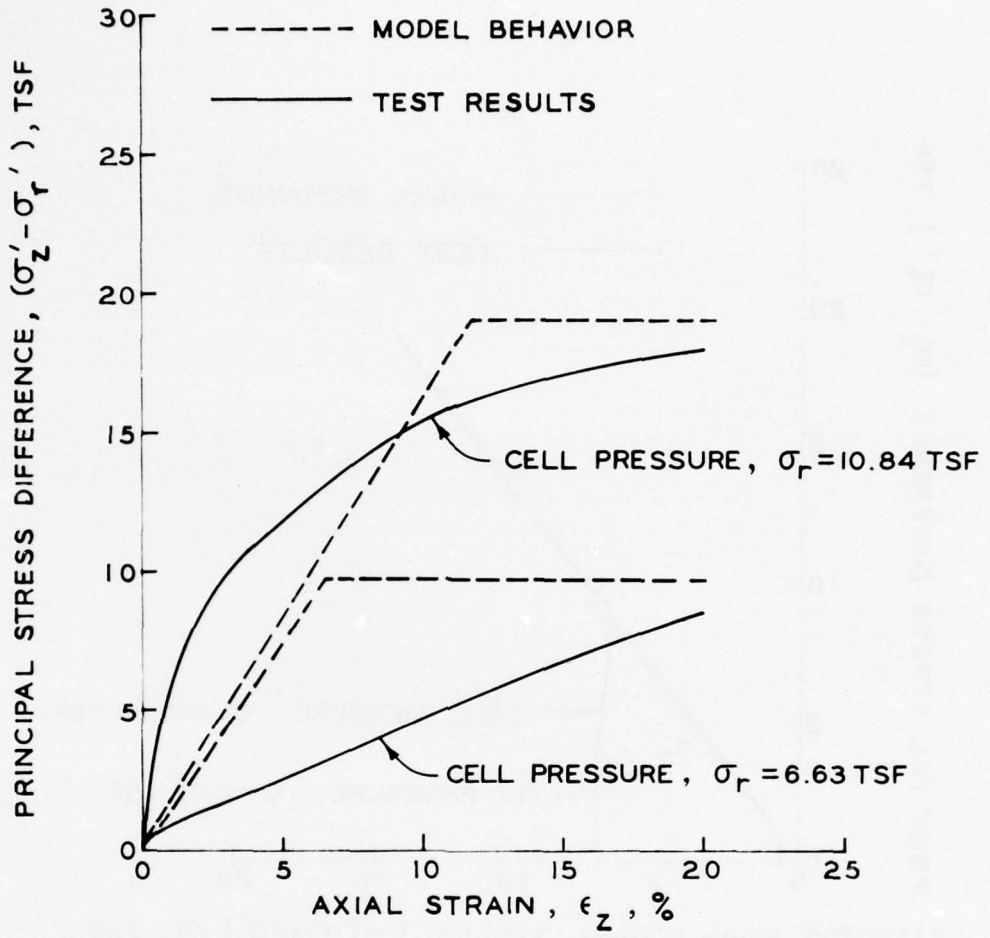

Figure 12. Comparison of principal stress difference vs axial strain relations produced by the model with test data for saturated Reid Bedford Model sand in undrained triaxial shear (Test Series 2)

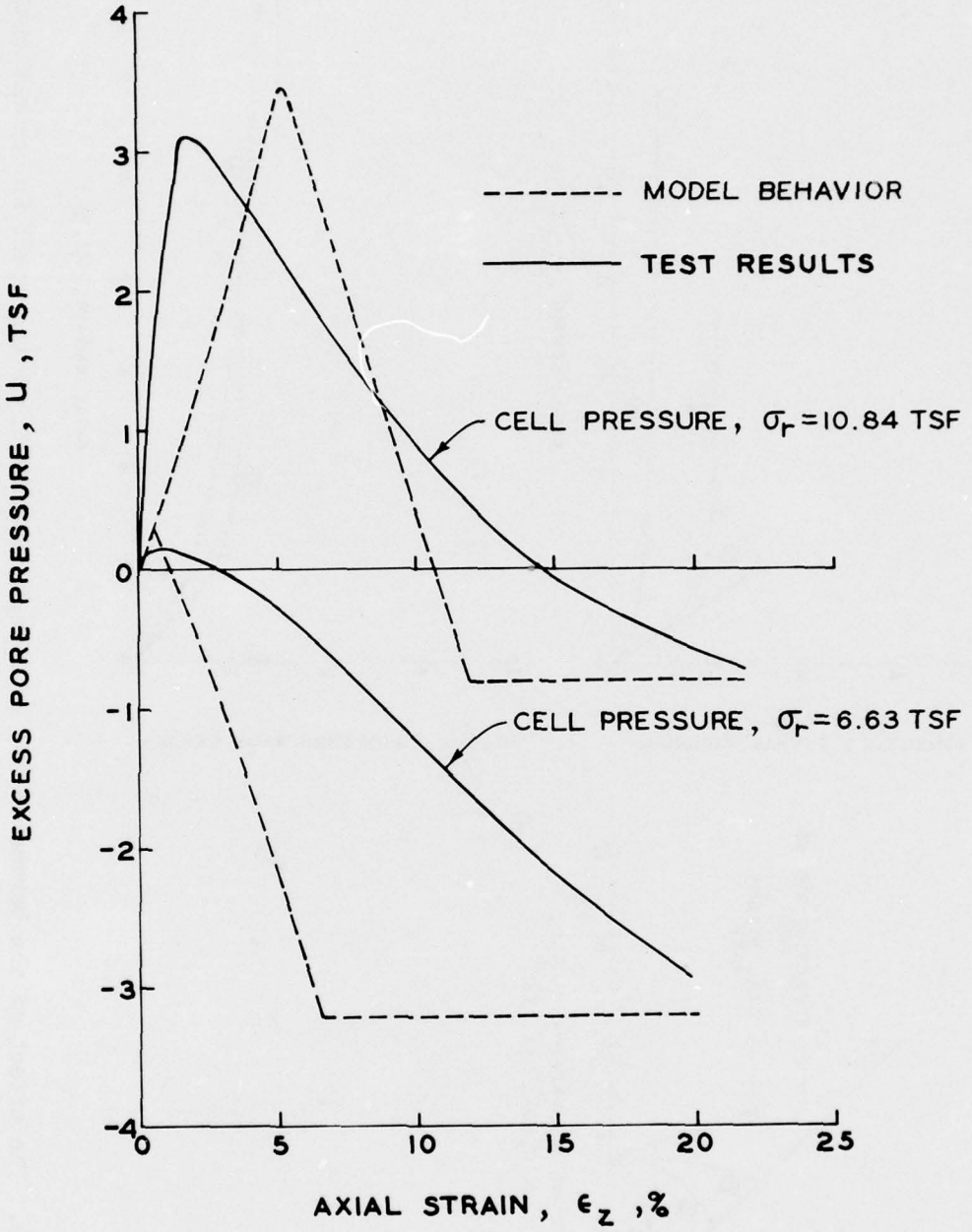

Figure 13. Comparison of excess pore water pressure vs axial strain produced by the model with test data for Reid Bedford Model sand in undrained triaxial shear (Test Series 2)

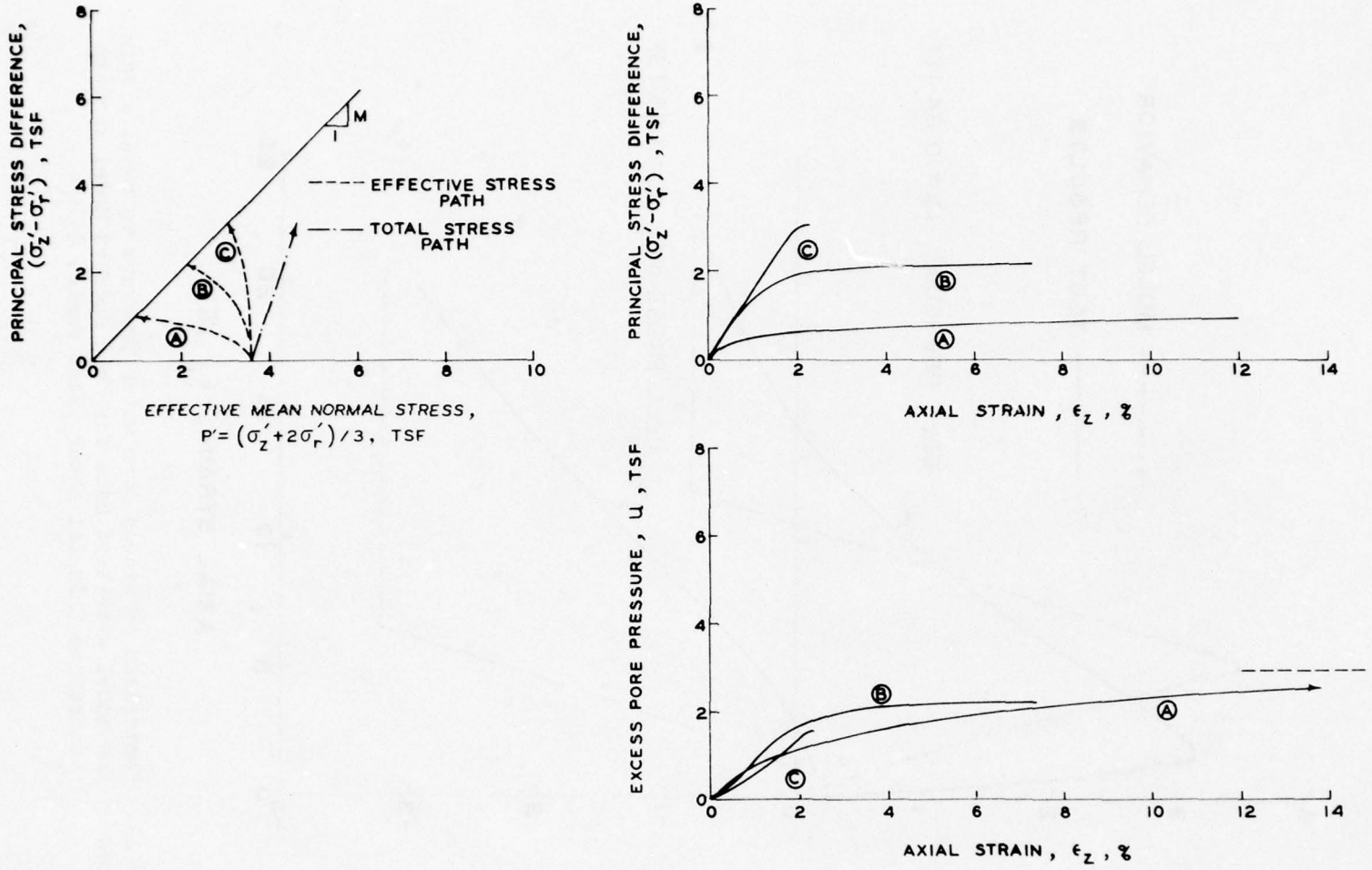

Figure 14. The effect of the parameter R on undrained behavior of the model in conventional triaxial test for a hypothetical material

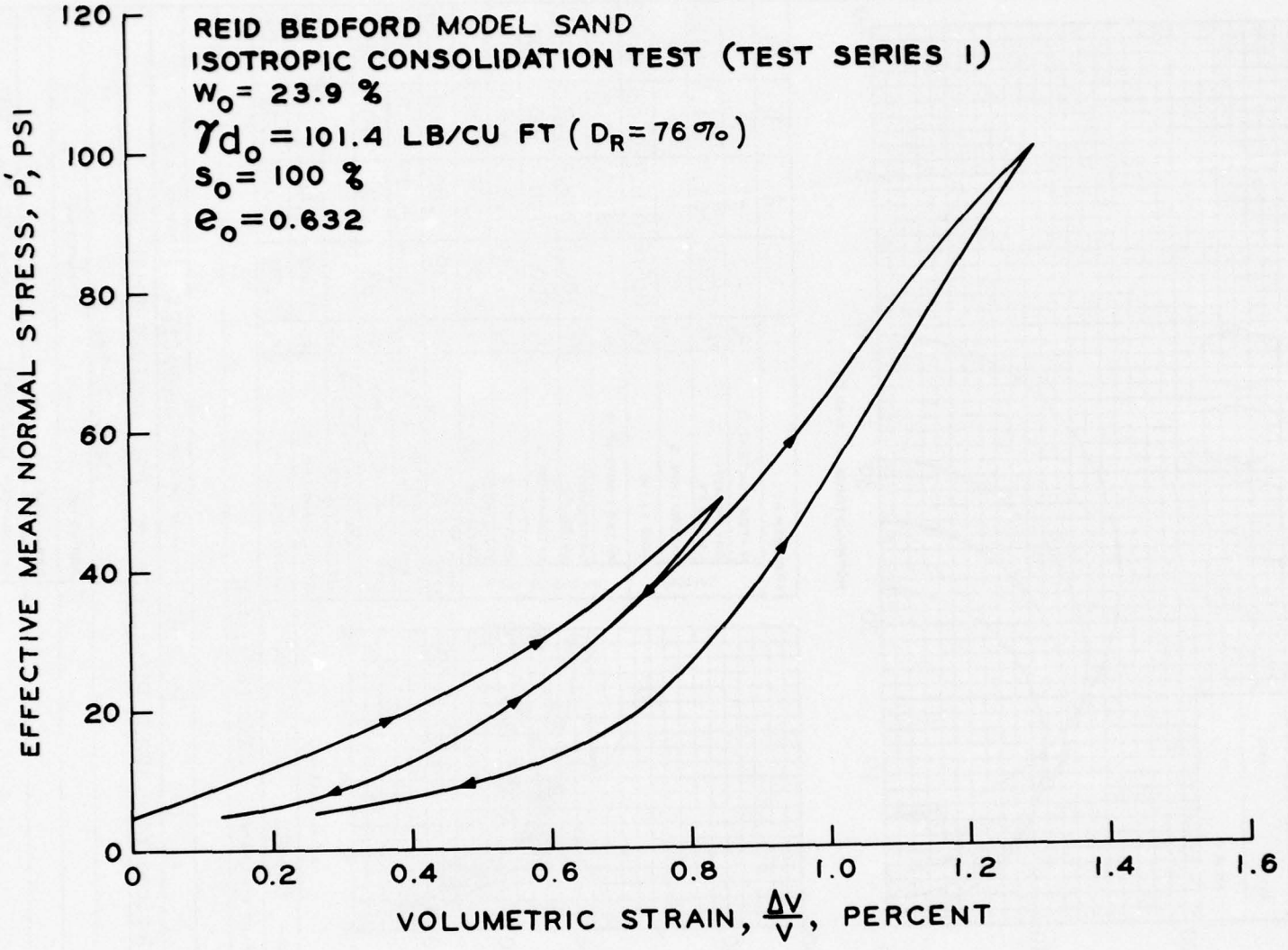
REID BEDFORD MODEL SAND
ISOTROPIC CONSOLIDATION TEST (TEST SERIES 1)
W_o= 23.9 %
γd_o = 101.4 LB/CU FT (D_R= 76 %)
S_o= 100 %
e_o=0.632
EFFECTIVE MEAN NORMAL STRESS, P', PSI
120
100
80
60
40
20
0
0
0.2
0.4
0.6
0.8
1.0
1.2
1.4
1.6
VOLUMETRIC STRAIN, $\frac{\Delta V}{V}$, PERCENT

PLATE 1

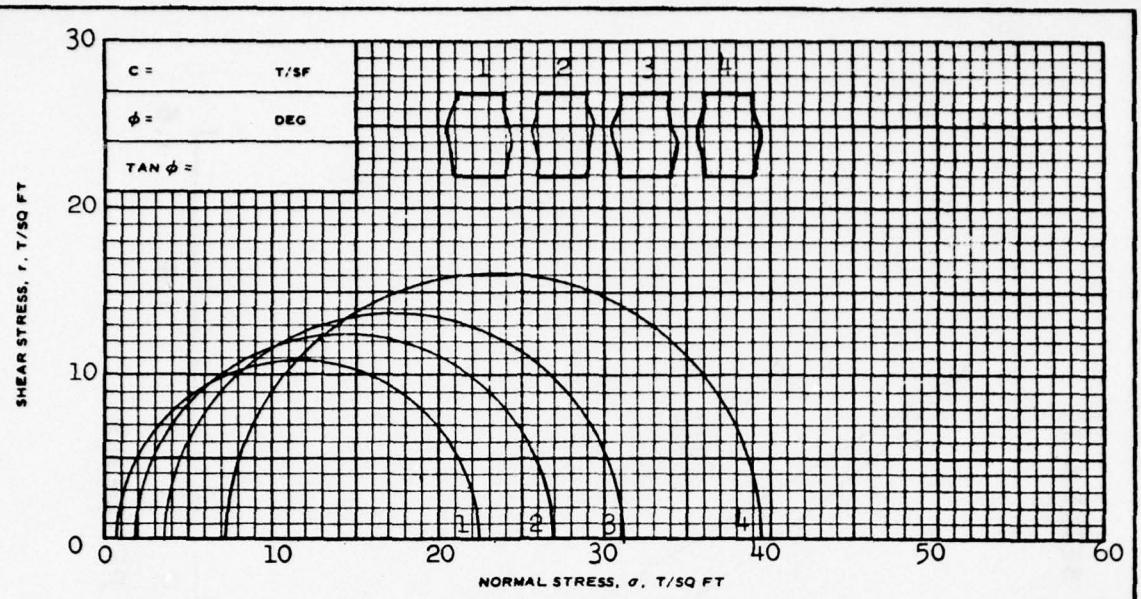

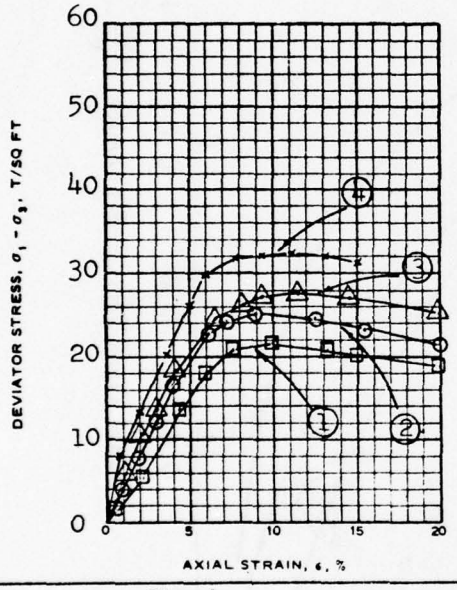

SPECIMEN NO.			1	2	3	4
INITIAL	WATER CONTENT, %	w_o	-	-	-	-
	DRY DENSITY LB/ CU FT	γ_{d_o}	102.4	101.7	101.4	101.4
	SATURATION, %	S_o	-	-	-	-
	VOID RATIO	e_o	0.616	0.627	0.632	0.632
BEFORE SHEAR	WATER CONTENT, %	w_c	23.2	23.7	23.9	23.9
	DRY DENSITY LB/CU FT	γ_{d_c}	102.7	102.4	102.5	102.7
	SATURATION, %	S_c	100	100	100	100
	VOID RATIO	e_c	0.611	0.615	0.615	0.611
	FINAL BACK PRESSURE, T/SQ FT	u_o	5.85	5.87	5.86	3.71
MINOR PRINCIPAL STRESS, T/SQ FT		σ_3	0.72	1.80	3.60	7.20
MAXIMUM DEVIATOR STRESS, T/SQ FT		$(\sigma_1 - \sigma_3)_{MAX}$	21.69	25.15	27.58	32.31
TIME TO $(\sigma_1 - \sigma_3)_{MAX}$, MIN		t_f	68	62	79	66
ULTIMATE DEVIATOR STRESS, T/SQ FT		$(\sigma_1 - \sigma_3)_{ULT}$				
INITIAL DIAMETER, IN.		D_o	1.40	1.40	1.40	1.40
INITIAL HEIGHT, IN.		H_o	2.99	3.01	3.03	3.03

CONTROLLED- Strain TEST

DESCRIPTION OF SPECIMENS SAND (SP), tan

LL -	PL -	PI -	G_s 2.65	TYPE OF SPECIMEN COMPACTED	TYPE OF TEST $\overline{R}$

REMARKS: Desired γd = 102.0 lb/cu.ft.

PROJECT Reid Bedford Model Sand
(Test Series 1)

BORING NO. - SAMPLE NO. -

DEPTH/ELEV -

LABORATORY USAEWES DATE 19 Feb. 1976

PJR TRIAXIAL COMPRESSION TEST REPORT

ENG FORM NO. 2089 REV JUNE 1970 PREVIOUS EDITION IS OBSOLETE TRANSLUCENT (EM 1110-2-1906)

PLATE 2

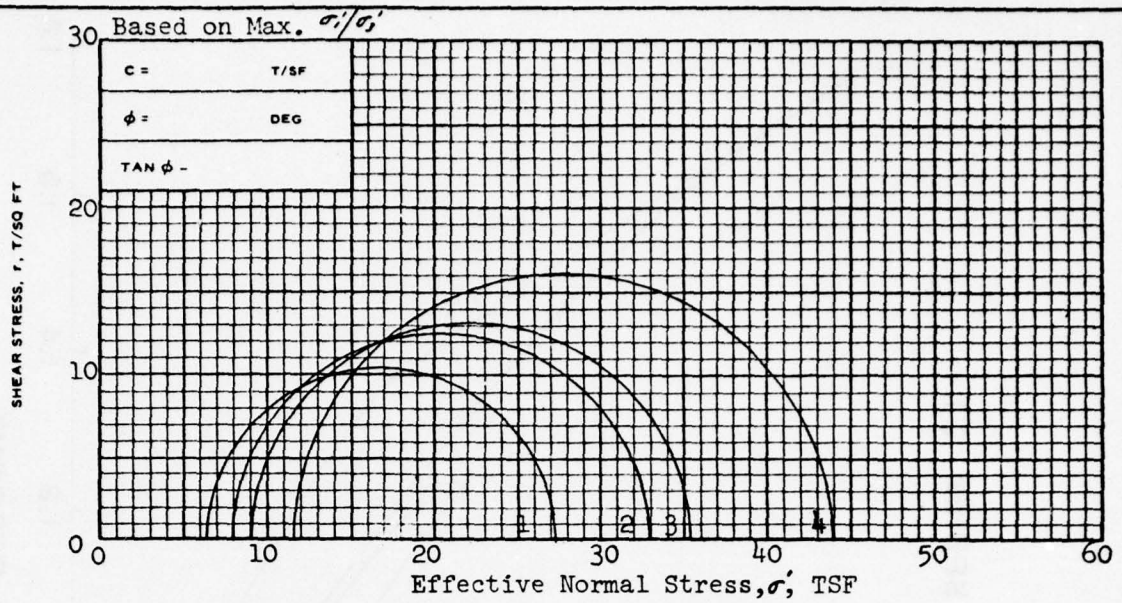

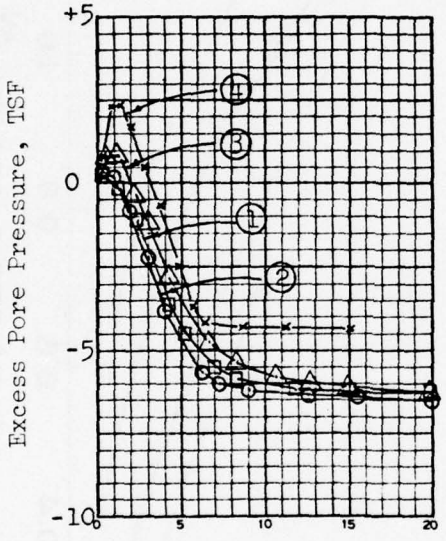

SPECIMEN NO.							
INITIAL	WATER CONTENT, %	w_o					
	DRY DENSITY LB/ CU FT	γ_{d_o}					
	SATURATION, %	S_o					
	VOID RATIO	e_o					
BEFORE SHEAR	WATER CONTENT, %	w_c					
	DRY DENSITY LB/CU FT	γ_{d_c}					
	SATURATION, %	S_c					
	VOID RATIO	e_c					
	FINAL BACK PRESSURE, T/SQ FT	u_o					
MINOR PRINCIPAL STRESS, T/SQ FT		σ_3					
MAXIMUM DEVIATOR STRESS, T/SQ FT		$(\sigma_1 - \sigma_3)_{MAX}$					
TIME TO $(\sigma_1 - \sigma_3)_{MAX}$, MIN		t_f					
ULTIMATE DEVIATOR STRESS, T/SQ FT		$(\sigma_1 - \sigma_3)_{ULT}$					
INITIAL DIAMETER, IN.		D_o					
INITIAL HEIGHT, IN.		H_o					

CONTROLLED- TEST

DESCRIPTION OF SPECIMENS

LL	PL	PI	G_s	TYPE OF SPECIMEN	TYPE OF TEST

REMARKS: Effective failure envelope is based on max. σ_1'/σ_3'

PROJECT Reid Bedford Model Sand (Test Series 1)

BORING NO. - SAMPLE NO. -

DEPTH/ELEV

LABORATORY USAEWES DATE 19 Feb. 1976

TRIAXIAL COMPRESSION TEST REPORT

ENG FORM NO. 2089 REV JUNE 1970 PREVIOUS EDITION IS OBSOLETE TRANSLUCENT (EM 1110-2-1906)

PLATE 3

PLATE 4

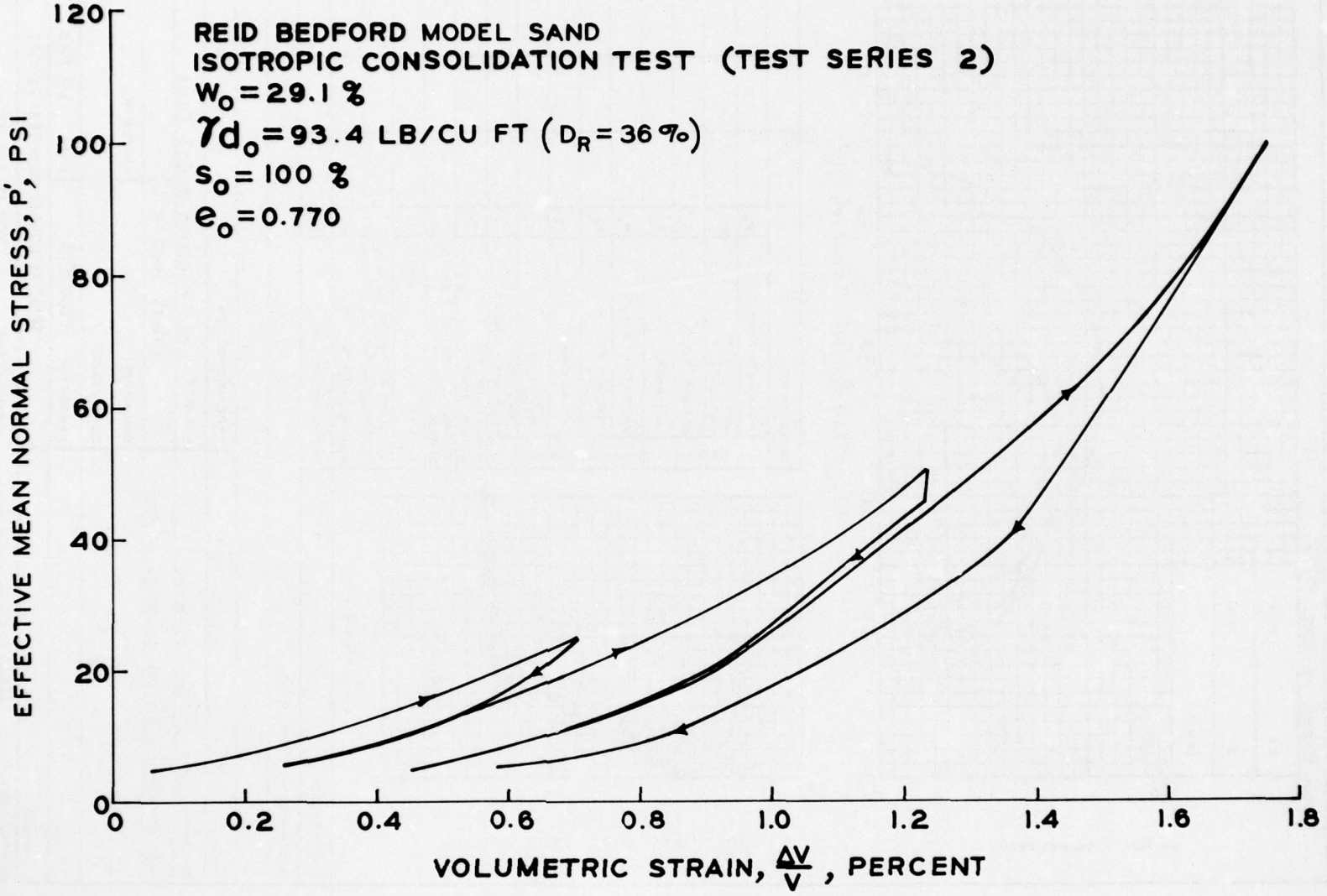
REID BEDFORD MODEL SAND
ISOTROPIC CONSOLIDATION TEST (TEST SERIES 2)
$W_o = 29.1\ \%$
$\gamma d_o = 93.4$ LB/CU FT ($D_R = 36\%$)
$S_o = 100\ \%$
$e_o = 0.770$
EFFECTIVE MEAN NORMAL STRESS, P', PSI
0
20
40
60
80
100
120
0
0.2
0.4
0.6
0.8
1.0
1.2
1.4
1.6
1.8
VOLUMETRIC STRAIN, $\frac{\Delta V}{V}$, PERCENT

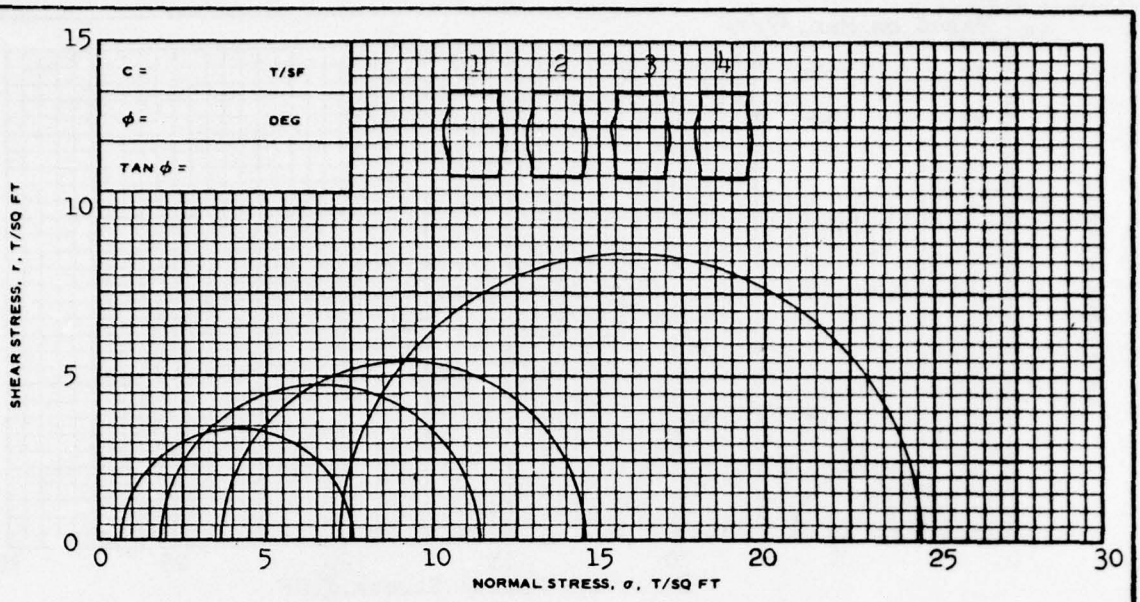

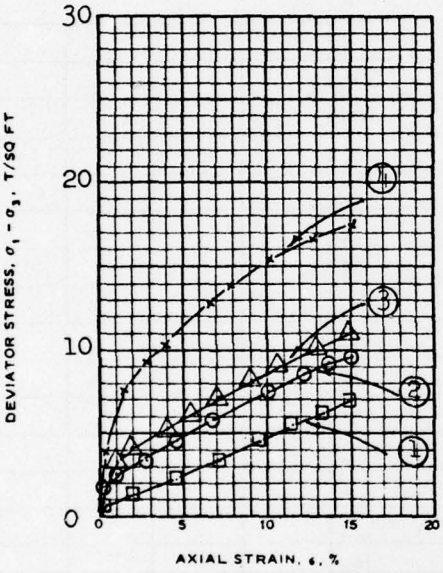

SPECIMEN NO.			1	2	3	4
INITIAL	WATER CONTENT, %	w_o	-	-	-	-
	DRY DENSITY LB/ CU FT	γ_{d_o}	93.5	94.0	93.4	93.4
	SATURATION, %	S_o	-	-	-	-
	VOID RATIO	e_o	0.769	0.759	0.770	0.770
BEFORE SHEAR	WATER CONTENT, %	w_c	27.5	27.0	27.2	26.8
	DRY DENSITY LB/CU FT	γ_{d_c}	94.3	95.1	94.9	95.3
	SATURATION, %	S_c	100	100	100	100
	VOID RATIO	e_c	0.754	0.740	0.744	0.736
	FINAL BACK PRESSURE, T/SQ FT	u_o	5.91	10.92	3.74	3.64
MINOR PRINCIPAL STRESS, T/SQ FT		σ_3	0.72	1.80	3.60	7.20
MAXIMUM DEVIATOR STRESS, T/SQ FT		$(\sigma_1 - \sigma_3)_{MAX}$	6.89	9.63	11.01	17.36
TIME TO $(\sigma_1 - \sigma_3)_{MAX}$, MIN		t_f	107	106	107	107
ULTIMATE DEVIATOR STRESS, T/SQ FT		$(\sigma_1 - \sigma_3)_{ULT}$				
INITIAL DIAMETER, IN.		D_o	1.40	1.39	1.39	1.39
INITIAL HEIGHT, IN.		H_o	3.07	3.07	3.09	3.09

CONTROLLED- Strain TEST

DESCRIPTION OF SPECIMENS SAND(SP), tan

LL - | PL - | PI - | G_s 2.65

TYPE OF SPECIMEN COMPACTED | TYPE OF TEST R

REMARKS: Desired γ_d= 95.0 lb/cu.ft.

PROJECT Reid Bedford Model Sand
(Test Series 2)

BORING NO. - | SAMPLE NO. -

DEPTH/ELEV - -

LABORATORY USAEWES | DATE 24 March 1976

PJR TRIAXIAL COMPRESSION TEST REPORT

ENG FORM NO. 2089 REV JUNE 1970 PREVIOUS EDITION IS OBSOLETE TRANSLUCENT (EM 1110-2-1906)

PLATE 5

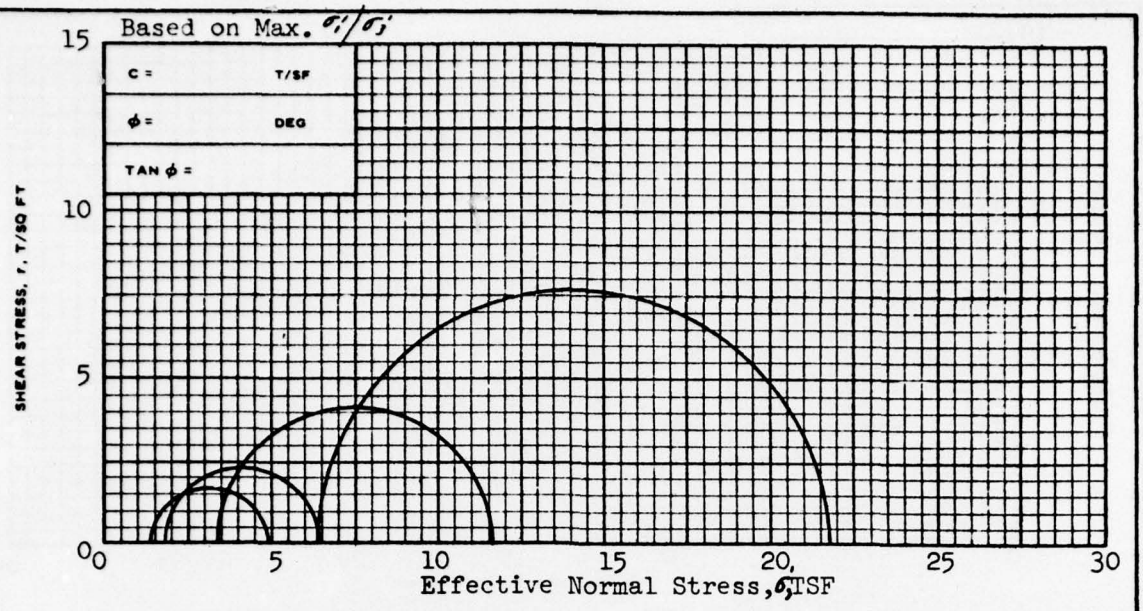

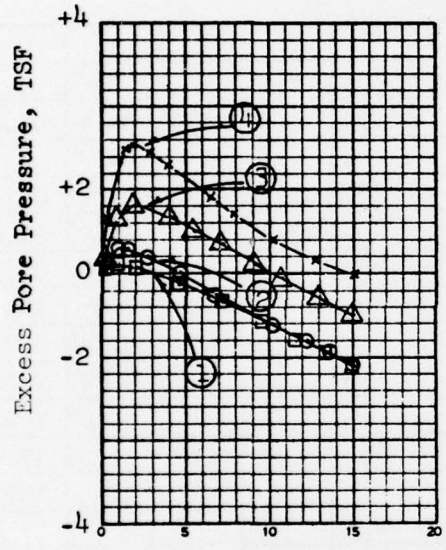

SPECIMEN NO.						
INITIAL	WATER CONTENT, %	w_o				
	DRY DENSITY LB/ CU FT	γ_{d_o}				
	SATURATION, %	S_o				
	VOID RATIO	e_o				
BEFORE SHEAR	WATER CONTENT, %	w_c				
	DRY DENSITY LB/CU FT	γ_{d_c}				
	SATURATION, %	S_c				
	VOID RATIO	e_c				
	FINAL BACK PRESSURE, T/SQ FT	u_o				
MINOR PRINCIPAL STRESS, T/SQ FT		σ_3				
MAXIMUM DEVIATOR STRESS, T/SQ FT		$(\sigma_1 - \sigma_3)_{MAX}$				
TIME TO $(\sigma_1 - \sigma_3)_{MAX}$, MIN		t_f				
ULTIMATE DEVIATOR STRESS, T/SQ FT		$(\sigma_1 - \sigma_3)_{ULT}$				
INITIAL DIAMETER, IN.		D_o				
INITIAL HEIGHT, IN.		H_o				

CONTROLLED- TEST

DESCRIPTION OF SPECIMENS

LL	PL	PI	G_s

TYPE OF SPECIMEN

TYPE OF TEST

REMARKS: Effective failure envelope is based on max. σ_1'/σ_3'

PROJECT Reid Bedford Model Sand (Test Series 2)

BORING NO. - SAMPLE NO. -

DEPTH/ELEV - -

LABORATORY USAEWES DATE 24 March 1976

TRIAXIAL COMPRESSION TEST REPORT

ENG FORM NO. 2089 REV JUNE 1970 PREVIOUS EDITION IS OBSOLETE TRANSLUCENT (EM 1110-2-1906)

PLATE 6

APPENDIX A

FUNDAMENTAL BASIS OF ELASTIC-PLASTIC MATERIAL MODELS

Basic Concepts From Continuum Mechanics

1. In engineering practice it is convenient, and often reasonable, to disregard the structural details of materials and consider their gross behavior only. Engineering materials are therefore described, or characterized, mathematically within the frameworks of the theory of continuous mass media. Neglecting thermal effects, the basic field equations that govern the motion of a continuum are the continuity equation*

$$\frac{\partial \rho}{\partial t} + (\rho\, v_i)_{,i} = 0 \tag{A1}$$

and the equations of motion

$$\sigma_{ij,j} + F_i - \rho a_i = 0 \tag{A2}$$

where

ρ = mass density

t = time

v_i = components of velocity vector

σ_{ij} = symmetrical stress tensor

F_i = components of body force

a_i = components of acceleration vector

2. Equations A1 and A2 constitute four equations that involve ten unknown functions of time and space: the mass density ρ, the three velocity components v_i, and the six independent stress components σ_{ij}.

---

* Indices take on values 1, 2, or 3. A repeated index is to be summed over its range. Comma in the subscripts represents a derivative. Quantities are referred to rectangular Cartesian coordinates X_i.

The body force components F_i are known quantities and the acceleration components a_i are expressible in terms of the velocity components v_i. Therefore, six additional equations relating the ten unknown variables are required in order to determine the motion or deformation of a medium when subjected to external disturbances such as surface forces and/or displacements. In continuum mechanics, such relations are stated by constitutive equations (or material models), which relate stresses to deformation and history of deformation. The difference between constitutive equations and field equations (Equations A1 and A2) is that the latter are applicable to all materials, whereas the former represent the intrinsic response of a particular material or class of materials.

3. The general form of a constitutive equation may be expressed by the functional form

$$g_{ab}\,(D_{mn}\,,\ \varepsilon_{rs}\,,\ \Omega_{qp}\,,\ \sigma_{ij}\,,\ \rho) = 0 \tag{A3}$$

where the deformation-rate and spin tensors, D_{mn} and Ω_{qp}, respectively, are related to the components of the velocity vector v_i

$$\begin{aligned} D_{mn} &= \frac{1}{2}\,(v_{m,n} + v_{n,m}) \\ \Omega_{pq} &= \frac{1}{2}\,(v_{p,q} - v_{q,p}) \end{aligned} \tag{A4}$$

and the strain tensor ε_{rs} is related to the components of displacement vector u_i. For small displacement gradients

$$\varepsilon_{rs} = \frac{1}{2}\,(u_{r,s} + u_{s,r}) \tag{A5}$$

Equations A1 through A3 constitute ten equations which include ten unknown variables. These equations will lead, in conjunction with the kinematic relations given by Equations A4 and A5 and boundary conditions, to a complete description for solution of a boundary-value problem.

4. The mechanical behavior of a number of engineering materials is described within the framework of elastic-plastic constitutive relationships. The development of the specific functional form of Equation A3 for the elastic-plastic models is given in the following section.

General Description of Elastic-Plastic Constitutive Models

5. The basic premise of elastic-plastic constitutive models is the assumption that certain materials are capable of undergoing small plastic (permanent) as well as elastic (recoverable) strains at each loading increment. Mathematically, the total strain increment is assumed to be the sum of the elastic and plastic strain increments, i.e.,

$$d\varepsilon_{ij} = d\varepsilon^{E}_{ij} + d\varepsilon^{P}_{ij} \tag{A6}$$

where

$d\varepsilon_{ij}$ = components of the total strain increment tensor

$d\varepsilon^{E}_{ij}$ = components of the elastic strain increment tensor

$d\varepsilon^{P}_{ij}$ = components of the plastic strain increment tensor

6. Within the elastic range the behavior of the material can be described by an elastic constitutive relation of the type

$$d\varepsilon^{E}_{ij} = A_{ijkl}\,(\sigma_{mn})\,d\sigma_{kl} \tag{A7}$$

where

A_{ijkl} = material response function

$d\sigma_{kl}$ = components of stress increment tensor

The behavior of the material in the plastic range can be described within the framework of the generalized incremental theory of plasticity. The mathematical basis of the theory was established by Drucker[12*] by

---

* Raised numerals refer to similarly numbered items in the References at the end of the main text.

introducing the concept of material stability with the following implications:

(a) yield surface (loading function) should be convex in stress space

(b) yield surface and plastic potential should coincide (this is referred to as associated flow rule)

(c) work "softening" should not occur

These three conditions can be summarized mathematically by the following inequality

$$d\sigma_{ij} \; d\varepsilon^{P}_{ij} \geq 0 \tag{A8}$$

The above conditions allow considerable flexibility in choosing the form of the loading function (f) for the model, which serves as both a yield surface and plastic potential. For isotropic materials the yield surface may be expressed, for example, as

$$f\,(J_1\,, \sqrt{\bar{J}_2}\,, \kappa) = 0 \tag{A9}$$

where

$J_1 = \sigma_{nn}$ = first invariant of stress tensor

$\bar{J}_2 = \frac{1}{2} S_{ij} S_{ij}$ = second invariant of stress deviation tensor

$S_{ij} = \sigma_{ij} - (J_1/3)\,\delta_{ij}$ = stress deviation tensor

$$\delta_{ij} = \begin{cases} 1 & i = j \\ 0 & i \neq j \end{cases} \quad = \text{Kronecker delta}$$

κ = a hardening parameter

The hardening parameter κ, in general, can be taken to be a function of plastic strain tensor ε^{P}_{ij}. The yield surface of Equation A9 may expand or contract as the hardening parameter κ increases or decreases, respectively (Figure A1).

7. Conditions a, b, and c above, taken in conjunction with Equation A9, result in the following plastic flow rule for isotropic materials

$$d\varepsilon_{ij}^{P} = \begin{cases} d\lambda \dfrac{\partial f}{\partial \sigma_{ij}} & \text{if } f = 0 \\ 0 & \text{if } f < 0 \end{cases} \tag{A10}$$

where $d\lambda$ is a positive scalar factor of proportionality, which is non-zero only when plastic deformations occur, and is dependent on the particular form of the loading function.

Elastic strain increment tensor

8. For isotropic elastic materials strain increment tensor (Equation A7) takes the following form

$$d\varepsilon_{ij}^{E} = \frac{\delta_{ij}}{9K} dJ_1 + \frac{1}{2G} dS_{ij} \tag{A11}$$

where

K = elastic bulk modulus

G = elastic shear modulus

The bulk and shear moduli can be functions of the invariants of stress tensor. Accordingly, we will assume that $K = K(J_1, \bar{J}_2, \bar{J}_3)$ and $G = G(J_1, \bar{J}_2, \bar{J}_3)$ where $\bar{J}_3$ is the third invariant of stress deviation tensor. Equation A11 can be written in terms of the hydrostatic and deviatoric components of strain and stress increment tensors, i.e.,

$$d\varepsilon_{kk}^{E} = \frac{1}{3K(J_1, \bar{J}_2, \bar{J}_3)} dJ_1 \tag{A12}$$

$$de_{ij}^{E} = \frac{1}{2G(J_1, \bar{J}_2, \bar{J}_3)} dS_{ij} \tag{A13}$$

where

$d\varepsilon_{kk}^{E}$ = increment of elastic volumetric strain

de_{ij}^{E} = elastic strain deviation increment tensor

In order not to generate energy or hysteresis within the elastic range, the elastic behavior of the model must be path independent. The material should then possess a positive definite elastic internal energy function (W) which is independent of stress path. The strain energy function can be written as

$$
\begin{aligned}
W &= \int_0^{\varepsilon_{ij}} \sigma_{ij}\, d\varepsilon_{ij} \\
&= \int_0^{\sigma_{ij}} (S_{ij} + \tfrac{1}{3} J_1\, \delta_{ij}) \left[\frac{dJ_1}{9K\,(J_1\,,\,\bar{J}_2\,,\,\bar{J}_3)}\, \delta_{ij} + \frac{dS_{ij}}{2G\,(J_1\,,\,\bar{J}_2\,,\,\bar{J}_3)} \right] \\
&= \int_0^{J_1} \frac{J_1}{9K\,(J_1\,,\,\bar{J}_2\,,\,\bar{J}_3)}\, dJ_1 + \int_0^{S_{ij}} \frac{1}{2G\,(J_1\,,\,\bar{J}_2\,,\,\bar{J}_3)}\, S_{ij}\, dS_{ij} \\
&= \int_0^{J_1} \frac{d(J_1)^2}{18K\,(J_1\,,\,\bar{J}_2\,,\,\bar{J}_3)} + \int_0^{\bar{J}_2} \frac{d\bar{J}_2}{2G\,(J_1\,,\,\bar{J}_2\,,\,\bar{J}_3)}
\end{aligned}
\tag{A14}
$$

In order for W to be independent of stress path, the integrals in Equation A14 have to depend only on the current values of J_1 and $\bar{J}_2$. Therefore, the bulk and shear moduli have to be expressed as

$$
\begin{aligned}
K &= K\,(J_1) \\
G &= G\,(\bar{J}_2)
\end{aligned}
\tag{A15}
$$

Further, K and G must always be positive. Since during elastic deformation the hardening parameter (κ) is constant, the bulk and shear moduli can also be expressed as

$$
\begin{aligned}
K &= K\,(J_1\,,\,\kappa) \\
G &= G\,(\bar{J}_2\,,\,\kappa)
\end{aligned}
\tag{A16}
$$

Plastic strain increment tensor

9. The plastic strain increment tensor is given by Equation A10 where the loading function f is given by Equation A9. The hardening function in Equation A9 could be taken as being equal to plastic volumetric strain ε^{P}_{kk}, thus

$$\kappa = \varepsilon^{P}_{kk} \tag{A17}$$

The use of Equation A17 will allow the yield surface to expand as well as to contract, Figure A1. The plastic loading criteria for the function f are given as

$$df = \frac{\partial f}{\partial \sigma_{ij}} d\sigma_{ij} \begin{cases} > 0 \text{ loading} \\ = 0 \text{ neutral loading} \\ < 0 \text{ unloading} \end{cases} \tag{A18}$$

Because $d\varepsilon^{P}_{ij} = 0$ during unloading or neutral loading, as well as for $f < 0$, Equations A11 through A13 are used to determine the purely elastic strain changes. The prescription that neutral loading produces no plastic strain is called the continuity condition. Its satisfaction leads to concidence of elastic and plastic constitutive laws during neutral loading.[12,13]

10. Like the elastic behavior, the plastic stress-strain relation can be expressed in terms of the hydrostatic and deviatoric components of strain. Applying the chain rule of differentiation to the right-hand side of Equation A10 yields

$$d\varepsilon_{ij}^{P} = d\lambda \left[\frac{\partial f}{\partial J_1} \frac{\partial J_1}{\partial \sigma_{ij}} + \frac{\partial f}{\partial \sqrt{J_2}} \frac{\partial \sqrt{J_2}}{\partial \sigma_{ij}} \right]$$

or

$$d\varepsilon_{ij}^{P} = d\lambda \left[\frac{\partial f}{\partial J_1} \delta_{ij} + \frac{1}{2\sqrt{J_2}} \frac{\partial f}{\partial \sqrt{J_2}} S_{ij} \right] \tag{A19}$$

Multiplying both sides of Equation A19 by δ_{ij} gives

$$d\varepsilon_{kk}^{P} = 3\, d\lambda \frac{\partial f}{\partial J_1} \tag{A20}$$

The deviatoric component of the plastic strain increment tensor (de_{ij}^{P}) can be written as

$$de_{ij}^{P} = d\varepsilon_{ij}^{P} - \frac{1}{3} d\varepsilon_{kk}^{P} \delta_{ij} \tag{A21}$$

Substitution of Equations A19 and A20 into Equation A21 yields

$$de_{ij}^{P} = \frac{d\lambda}{2\sqrt{J_2}} \frac{\partial f}{\partial \sqrt{J_2}} S_{ij} \tag{A22}$$

11. In order to use Equations A20 and A22, or Equation A19, the proportionality factor $d\lambda$ must be determined. This can be accomplished in the following manner. From Equations A9 and A17 the total derivative of f becomes

$$df = \frac{\partial f}{\partial J_1} dJ_1 + \frac{1}{2\sqrt{J_2}} \frac{\partial f}{\partial \sqrt{J_2}} S_{ij}\, dS_{ij} + \frac{\partial f}{\partial \varepsilon_{kk}^{P}} d\varepsilon_{kk}^{P} = 0 \tag{A23}$$

In view of Equations A12, A13, and A20, Equation A23 becomes

$$3K\, d\varepsilon_{kk}^{E} \frac{\partial f}{\partial J_1} + \frac{G\, de_{ij}^{E}}{\sqrt{J_2}} \frac{\partial f}{\partial \sqrt{J_2}} S_{ij} + 3\, d\lambda \frac{\partial f}{\partial J_1} \frac{\partial f}{\partial \varepsilon_{kk}^{P}} = 0 \tag{A24}$$

Substituting Equation A6 into Equation A24 results in

$$3K\,(d\varepsilon_{kk} - d\varepsilon^{P}_{kk})\,\frac{\partial f}{\partial J_1} + \frac{G}{\sqrt{J_2}}\,(de_{ij} - de^{P}_{ij})\,\frac{\partial f}{\partial \sqrt{J_2}}\,S_{ij} = -3\,d\lambda\,\frac{\partial f}{\partial J_1}\,\frac{\partial f}{\partial \varepsilon^{P}_{kk}} \qquad \text{(A25)}$$

or

$$3K\,d\varepsilon_{kk}\,\frac{\partial f}{\partial J_1} + \frac{G}{\sqrt{J_2}}\,\frac{\partial f}{\partial \sqrt{J_2}}\,S_{ij}de_{ij} = 3K\,d\varepsilon^{P}_{kk}\,\frac{\partial f}{\partial J_1} + \frac{G}{\sqrt{J_2}}\,\frac{\partial f}{\partial \sqrt{J_2}}\,S_{ij}de^{P}_{ij}$$

$$- 3\,d\lambda\,\frac{\partial f}{\partial J_1}\,\frac{\partial f}{\partial \varepsilon^{P}_{kk}} \qquad \text{(A26)}$$

Substituting the values of $d\varepsilon^{P}_{kk}$ and de^{P}_{ij} from Equations A20 and A22, respectively, into Equation A26, we obtain

$$3K\,d\varepsilon_{kk}\,\frac{\partial f}{\partial J_1} + \frac{G}{\sqrt{J_2}}\,\frac{\partial f}{\partial \sqrt{J_2}}\,S_{ij}de_{ij} = 9K\,d\lambda\,\left(\frac{\partial f}{\partial J_1}\right)^2 + G\,d\lambda\,\left(\frac{\partial f}{\partial \sqrt{J_2}}\right)^2$$

$$- 3\,d\lambda\,\frac{\partial f}{\partial J_1}\,\frac{\partial f}{\partial \varepsilon^{P}_{kk}} \qquad \text{(A27)}$$

Solving for $d\lambda$, we obtain

$$d\lambda = \frac{3K\,\frac{\partial f}{\partial J_1}\,d\varepsilon_{kk} + \frac{G}{\sqrt{J_2}}\,\frac{\partial f}{\partial \sqrt{J_2}}\,S_{ij}de_{ij}}{9K\,\left(\frac{\partial f}{\partial J_1}\right)^2 + G\,\left(\frac{\partial f}{\partial \sqrt{J_2}}\right)^2 - 3\,\frac{\partial f}{\partial J_1}\,\frac{\partial f}{\partial \varepsilon^{P}_{kk}}} \qquad \text{(A28)}$$

Total strain increment tensor

12. The total strain increment tensor can be obtained by combining Equations A6, A11, A19, and A28; thus,

$$d\varepsilon_{ij} = \frac{dJ_1}{9K}\,\delta_{ij} + \frac{dS_{ij}}{2G}$$

$$+\left[\frac{3K\,\frac{\partial f}{\partial J_1}\,d\varepsilon_{kk} + \frac{G}{\sqrt{J_2}}\,\frac{\partial f}{\partial \sqrt{J_2}}\,S_{mn}\,de_{mn}}{9K\left(\frac{\partial f}{\partial J_1}\right)^2 + G\left(\frac{\partial f}{\partial \sqrt{J_2}}\right)^2 - 3\,\frac{\partial f}{\partial J_1}\,\frac{\partial f}{\partial \varepsilon^P_{kk}}}\right]\left[\frac{\partial f}{\partial J_1}\,\delta_{ij} + \frac{1}{2\sqrt{J_2}}\,\frac{\partial f}{\partial \sqrt{J_2}}\,S_{ij}\right] \tag{A29}$$

Similarly, the stress increment tensor can be written as

$$d\sigma_{ij} = K\,d\varepsilon_{kk}\,\delta_{ij} + 2G\,de_{ij}$$

$$-\left[\frac{3K\,\frac{\partial f}{\partial J_1}\,d\varepsilon_{kk} + \frac{G}{\sqrt{J_2}}\,\frac{\partial f}{\partial \sqrt{J_2}}\,S_{mn}\,de_{mn}}{9K\left(\frac{\partial f}{\partial J_1}\right)^2 + G\left(\frac{\partial f}{\partial \sqrt{J_2}}\right)^2 - 3\,\frac{\partial f}{\partial J_1}\,\frac{\partial f}{\partial \varepsilon^P_{kk}}}\right]\left[3K\,\frac{\partial f}{\partial J_1}\,\delta_{ij} + 2G\,\frac{\partial f}{\partial \sqrt{J_2}}\,\frac{S_{ij}}{2\sqrt{J_2}}\right] \tag{A30}$$

Equation A29, or Equation A30, is the general constitutive equation for an elastic-plastic isotropic material. To use these equations it is only necessary to specify the functional forms of K, G, and f.

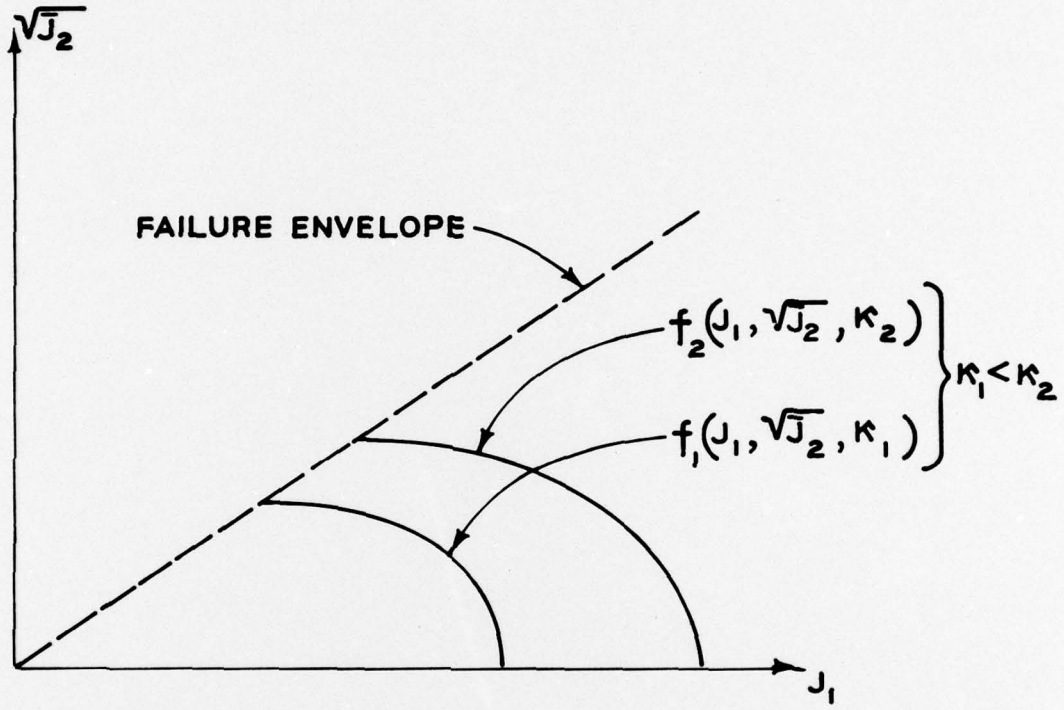

Figure A1. Typical yield surface for an elastic-plastic model

In accordance with ER 70-2-3, paragraph 6c(1)(b), dated 15 February 1973, a facsimile catalog card in Library of Congress format is reproduced below.

Baladi, George Y

Liquefaction potential of dams and foundations; Report 3: Development of an elastic-plastic constitutive relationship for saturated sand, by George Y. Baladi [and] Behzad Rohani. Vicksburg, U. S. Army Engineer Waterways Experiment Station, 1977.

1 v. (various pagings) illus. 27 cm. (U. S. Waterways Experiment Station. Research report S-76-2, Report 3)

Prepared for Office, Chief of Engineers, U. S. Army, Washington, D. C., under CWIS 31145.

Includes bibliography.

1. Constitutive relations. 2. Dams. 3. Foundations. 4. Liquefaction (Soils). 5. Sands. 6. Saturated soils. I. Rohani, Behzad, joint author. II. U. S. Army. Corps of Engineers. (Series: U. S. Waterways Experiment Station, Vicksburg, Miss. Research report S-76-2, Report 3)

TA7.W34r no.S-76-2 Report 3